Astronomy & Astrophysics manuscript no. output
May 22, 2023

Contribution of S-type asteroid families to NEOs and meteoroid populations

M. Brož[1], M. Marsset[2,3], P. Vernazza[4], F. DeMeo[3], R. Binzel[3], D. Vokrouhlický[1], and D. Nesvorný[5]

[1] Charles University, Faculty of Mathematics and Physics, Institute of Astronomy, V Holešovičkách 2, 18000 Prague, Czech Republic
[2] European Southern Observatory (ESO), Alonso de Cordova 3107, 1900 Casilla Vitacura, Santiago, Chile
[3] Department of Earth, Atmospheric and Planetary Sciences, MIT, 77 Massachusetts Avenue, Cambridge, MA 02139, USA
[4] Aix Marseille Univ, CNRS, LAM, Laboratoire d'Astrophysique de Marseille, Marseille, France
[5] Southwest Research Institute, 1050 Walnut Street, Suite 400, Boulder, CO 80302, USA

Received x-x-2023 / Accepted x-x-2023

ABSTRACT

Context. Previous spectroscopic observations of silicate-rich (S-type) near-Earth objects (NEOs) have revealed a significant discrepancy between the mineralogical distribution of these bodies and that of their meteorite counterparts, the ordinary chondrites (OCs). This points at different **sources of kilometre- and metre-sized** bodies that remain to be understood.
Aims. **In the accompanying paper by Marsset et al., an extensive spectroscopic survey of 976 NEOs was presented and a subset of S-type objects was analysed in detail. Their reflectance spectra were dereddened and linked to individual asteroid families as well as OCs, to determine the mineralogy (H, L, LL). In this work, we provide a context necessary to interpret these observations.**
Methods. We selected **11** major S-type families, namely: **Phocaea (H),** Maria (H), Merxia (H), Agnia (H), Koronis (L/H), Karin (L/H), **Massalia (L)**, Gefion (L), Juno (L/LL), Flora (LL), and Eunomia (LL). We identified their members using a recent catalogue of the proper elements (a_p, e_p, I_p), removed interlopers, and characterized the **size-frequency distributions** (SFDs) down to a 1-kilometre size. We then used a **statistical** collisional model, calibrated on Vesta (HED), to extrapolate the SFDs to a 1-metre size and to determine the ages from a characteristic slope change at about 5 km size. We used an orbital model **with the Yarkovsky and YORP effects** to transport bodies from the main belt and to determine the respective mean life times, which constrain the number of bodies in the NEO or meteoroid populations.
Results. The ages of asteroid families based on our collisional model (and literature data) range from 4200 My to 6 My. The contributions of individual families to the NEO and meteoroid populations vary in the course of time. Today, Flora, Vesta, **Phocaea**, Juno and Eunomia seem to be dominant for kilometre-sized bodies. The situation is more complex for metre-sized bodies though, with uncertainties stemming from a variable tail of the SFDs at small sizes. LL-chondrite-like and HED families contribute comparably (Flora $N_{neo}(>1\,m) = 6.3\text{-}12.5 \times 10^8$, Vesta $4.3\text{-}15.2 \times 10^8$), in agreement with observations. However, H- and L-chondrite-like **meteoroids** are under-represented compared to the observations **(by a factor of** $\sim$10); **other sources** must be dominant. Alternatively, the situation may be non-stationary, with non-zero derivatives $\dot{N}_{neo}(>1\,m)$. This is supported by **our** discovery of the Karin collisional series, composed of four sub-families within the Koronis family: Karin, Koronis$_{(2)}$, Koronis$_{(3)}$, and Koronis$_{(4)}$. Such events create a temporarily steep 'tail' of the SFD. **This is confirmed by the** 2.1° **dust band, observed by the Infrared Astronomical Telescope (IRAS).**
Conclusions. **In order to explain the dominant population of H- and L-chondrite-like meteoroids, several young families must be accounted for, namely the Karin series (for H), or the 2nd Massalia family (for L).**

Key words. Minor planets, asteroids: general – Earth – Celestial mechanics

1. Introduction

More than a decade ago, Vernazza et al. (2008) reported that the vast majority of objects that come near the Earth (NEOs) are spectrally alike LL ordinary chondrites (OCs), a type that matches only a tiny fraction of the meteorites most frequently hitting our planet (typically H and L chondrites). Subsequent studies confirmed these findings (Thomas & Binzel 2010; de León et al. 2010; Dunn et al. 2013). This may be called the meteorite–NEO conundrum.

A logical explanation of the meteorite–NEO conundrum is that different main-belt source regions may be responsible for supplying these two sample populations. In the case of km-sized NEOs, the inner asteroid belt appears as the most likely source region. This is both supported by spectroscopic observations of near-Earth and main belt asteroids (e.g., Vernazza et al. 2008, 2014; Marsset et al. 2022) and dynamical studies which show that $\approx$40% of all roughly kilometre-sized NEAs should be delivered from the asteroid belt to Earth-crossing orbits by the ν_6 resonance located on the innermost edge of the main belt (Bottke et al. 2002; Granvik et al. 2018). This is because objects originating from this resonance stay much longer in the NEO region than bodies originating from the remaining ones (3:1, 5:2, etc.).

These various resonance lifetimes **are assumed to also** apply to meteoroids in the $\approx$ 0.1 to 1 m size range, which is the typical size of pre-atmospheric meteorite parent bodies. This implies that meter-sized bodies entering the ν_6 resonance should have, in principle, a greater likelihood of reaching Earth's surface than meteoroids originating from elsewhere. If all contributions from the various main-belt regions (inner, middle and outer belt) were equal in terms of number of meter-sized bodies entering the various resonances, this would imply that the meteorite flux would

essentially originate from the inner belt which is in contradiction with the observed meteorite–NEO conundrum.

In essence, our meteorite collections would comprise many Flora-like (LL chondrites) and Vesta-like (HED meteorite) fragments, which is not the case as these two meteorite groups only represent $\approx 14\%$ of the recovered falls. This implies that there must be major sources of meter-sized fragment in the asteroid belt that remain to be identified and that overcome the number of meter-sized fragments produced by the Flora and Vesta families. Note that the background population, while certainly contributing to the meteorite flux, cannot be the main source of it as LL-like bodies are more abundant in the inner belt than H- or L-like bodies (Vernazza et al. 2014). It follows that a few 'large' stochastic collisional events should likely be the main source of the flux. Actually, this is exactly what CRE ages of H chondrites suggest (Graf & Marti 1995).

Here, we investigate the contributions of the largest S-type families to the current kilometre-size NEO population and metre-size NEO flux, as well as that of **some** smaller, recently formed (~ 10 My) S-type families **(Sect. 2)**. We use a collisional model to evaluate the size-frequency distribution of these families down to 1 m **(Sects. 3, 4)** and subsequently determine the NEO flux at **kilometre and metre** sizes from these families using **an orbital model (Sects. 5, 6)**.

2. Family identification

We used recent catalogues (Jun 2021) to identify families **for further modelling**. We combined the following datasets: Astorb (Moskovitz et al. 2019), AFP (Knežević & Milani 2003; Novaković & Radović 2019), Wise (Nugent et al. 2015), Akari (Usui et al. 2011), and SDSS (Parker et al. 2008), to obtain both orbital and physical data, whenever available. We used the hierarchical clustering method (HCM; Zappalà et al. 1995) on proper orbital elements with a variable cut off velocity as the initial step, followed by an addition of halo (optional), and a removal of interlopers. This is based on physical data; unless specified otherwise, we assumed the geometric albedo $p_V \in (0.1; 0.5)$ and the Sloan colour index $a^\star \in (-0.1; 0.5)$. Additionally, we used the relation between the absolute magnitude H and the proper semimajor axis a_p (Vokrouhlický et al. 2006b):

$$H(a_\mathrm{p}) = 5 \log_{10} \frac{|a_\mathrm{p} - a_\mathrm{c}|}{C}\,, \tag{1}$$

where the parameter C determines the overall extent of the family. Bodies are removed if $H < H(a_\mathrm{p})$. The value of C is directly related to the upper limit for the age (but *not* to the age; Nesvorný et al. 2015):

$$t_\uparrow = 1\,\mathrm{Gy}\,\frac{C}{10^{-4}\,\mathrm{au}}\left(\frac{a_\mathrm{c}}{2.5\,\mathrm{au}}\right)^2 \frac{\rho}{2.5\,\mathrm{g\,cm^{-3}}}\left(\frac{0.2}{p_V}\right)^{1/2}\,. \tag{2}$$

Technical intermezzo. The Vesta family was associated at 100 m/s (core) and 100 m/s (halo). For the first step, we used only bodies with $H \leq 15$ mag, for the second step $H > 15$ mag, so that the family is well separated from other families. Other parameters were: $a_\mathrm{c} = 2.36151$ au, $C = 3.0 \times 10^{-4}$ au, $p_V \in (0.1; 0.7)$, $a^\star \in (0; 0.5)$, $i - z \in (-0.85; -0.05)$. We considered (306) Unitas to be an interloper.

The Massalia family was associated at 30 m/s (core) and 100 m/s (halo); with $a_\mathrm{c} = 2.40863$ au, $C = 0.3 \times 10^{-4}$ au, $p_V \in (0.12; 0.6)$. It was a difficult case, because it is close to the Nysa/Polana complex and the 1:2 mean-motion resonance with Mars, which connects the two neighbouring families.

The Maria family was a simple case: $v = 55$ m/s, $a_\mathrm{c} = 2.55370$ au, $C = 2.3 \times 10^{-4}$ au.

The Merxia family too: $v = 50$ m/s; with $a_\mathrm{c} = 2.74513$ au, $C = 0.5 \times 10^{-4}$ au.

For the Agnia family, we had to choose a different central body (1020) Arcadia, located in the densest part, not (847) Agnia itself. The cut off velocities were 60 m/s (core), 80 m/s (halo); together with $a_\mathrm{c} = 2.79024$ au, $C = 0.17 \times 10^{-4}$ au. The family has a structure strongly affected by the z_1 secular resonance, along which the HCM associates bodies (Vokrouhlický et al. 2006a).

The Koronis family was associated at 55 m/s, and $a_\mathrm{c} = 2.86878$ au, $C = 4.3 \times 10^{-4}$ au. The family was extended beyond 2.96 au, i.e., the 7:3 mean-motion resonance with Jupiter, which fits well within the (a_p, H) envelope.

The Gefion family was a simple case: $v = 40$ m/s, $a_\mathrm{c} = 2.78381$ au, $C = 10^{-4}$ au.

The Juno family too: $v = 40$ m/s, $a_\mathrm{c} = 2.66938$ au, $C = 10^{-4}$ au.

For the Flora family, we used a 15-mag core at 110 m/s and a 20-mag halo at 100 m/s. Other parameters were $a_\mathrm{c} = 2.20145$ au, $C = 2.1 \times 10^{-4}$ au, $p_V \in (0.12; 0.6)$, $a^\star \in (0; 0.5)$, $i - z \in (-0.3; 0.5)$. It has a structure affected by the ν_6 secular resonance. Moreover, there is a persisting contamination from the Baptistina family.

The Eunomia family was associated at 40 m/s; with $a_\mathrm{c} = 2.64357$ au, $C = 2.3 \times 10^{-4}$ au. The (173) Ino family may be a part of Eunomia, just behind the 8:3 resonance. Possibly, this is also the case of (53546) 2000 BY_6.

All families as they were identified are shown in Fig. E.1. In order to compute diameters from magnitudes, we used either the measured albedos, or the median albedo of the respective families. The resulting SFDs are shown in Fig. 1.

Main belt population at 1 kilometre. We can directly compare the main-belt populations at 1 km, using a straightforward extrapolation from multi-kilometre sizes, because new data allowed us to actually see the observational bias. It affects the SFDs substantially at sub-km sizes for S-type populations, but at 1-km it can be 'safely' extrapolated from multi-kilometer sizes (Hendler & Malhotra 2020). Approximate slopes derived for observed SFDs are listed in Tab. 1. For H-chondrite families (see Fig. 1, left), the sequence from major to minor populations is (in 10^3 units):

Koronis (9.2) → Maria (5.5) → Agnia (3.1) → Phocaea (2.7) → Merxia (2.0) → Karin (1.1);

where we also included the Karin family (to be discussed in Sec. 8). For L-chondrite (middle):

Koronis (9.2) → **Juno** (4.2) → Gefion (3.8) → Massalia (2.6) → Karin (1.1);

for LL-chondrite (right):

Flora (7.2) → Eunomia (7.0) → **Juno** (4.2),

where some families are partly H, L, or LL. Contrary to our expectations, these 'borderline' families (Koronis, Juno) do have a potential to contribute substantially, especially to the H- and L-chondrite populations

On the other hand, a simple extrapolation of SFDs down to 1 metre is not possible and we need a collisional model to do this properly.

Table 1. Power-law slopes of the observed SFDs of the S-type families.

family	q_1	q_2	q_3
Vesta (HED)	−4.6	−3.3	−1.5
Phocaea (H)	−2.7	−1.4	
Maria (H)	−2.0	−2.7	−1.5
Merxia (H)	−3.2	−2.5	
Agnia (H)	−3.2	−2.9	
Koronis (L/H)	−2.5	−1.5	
Karin (L/H)	−4.2	−2.9	
Massalia (L)	−5.7	−3.4	−2.8
Gefion (L)	−3.9	−1.7	−1.1
Juno (L/LL)	−2.8	−3.7	−3.1
Flora (LL)	−3.8	−2.8	−1.3
Eunomia (LL)	−4.5	−3.2	−1.2

3. Calibration of the collisional model

We used the collisional code called Boulder (Morbidelli et al. 2009), which is a Monte-Carlo approach, working with binned differential mass distributions of an arbitrary number of populations. In our case, we used 3 populations: the main belt, one of the families and the NEO population. The Boulder code uses a number of parameters or relations describing how collisions between targets and projectiles produce fragments. The principal parameter is the critical impact specific energy $Q^\star(D)$ (in $\mathrm{J\,kg^{-1}}$), a function of the target size D. We used the formulation of Benz & Asphaug (1999) with modified parameters (as shown in Fig. 2):

$$Q^\star(D) = Q_0\,(D/2)^a + B\rho\,(D/2)^b\,, \tag{3}$$

where $Q_0 = 9\times10^7$, $a = -0.53$, $B = 0.5$, $b = 1.36$ (all in cgs units when applicable). **The density ρ was either** $3\,\mathrm{g\,cm^{-3}}$**, or specific (if known precisely).** These parameters are within the range of values tested by Bottke et al. (2020). Furthermore, relations for the largest remnant mass $M_{\mathrm{lr}}(Q)$, the largest fragment mass $M_{\mathrm{lf}}(Q)$, the slope of fragment size distribution $q(Q)$ are needed, where Q denotes the impact specific energy (also in $\mathrm{J\,kg^{-1}}$), as usually scaled by $Q^\star(D)$. For 100- and 10-km bodies, we used the relations described in Vernazza et al. (2018); Ševeček et al. (2017), with a linear interpolation in between. The collisional probabilities and velocities for various combinations of populations are listed in Table D.1. Because the evolution is stochastic, we always compute multiple (at least 10) runs to reject rare events (e.g., Ceres catastrophic disruptions).

Our collisional model is constrained by: (i) the observed main belt SFD (Bottke et al. 2015), (ii) the NEO SFD (Harris et al. 2015), (iii) the Vesta family SFD, (iv) Rheasylvia basin age 1 Gy (O'Brien et al. 2014), and (iv) (4) Vesta cratering record (Marchi et al. 2012), namely the heavily-cratered terrain (HCT) and the large diffuse craters (LDC). The final state of the model is shown in Fig. 4. As mentioned above, the $Q^\star(D)$ was adjusted in order to fit the *tail* of the observed main belt SFD, otherwise, synthetic populations 'undershoots' the observed one (see Fig. 2).

We use a full transport matrix between all populations. In fact, a transport is a complex process, driven by the Yarkovsky drift, the YORP effect, collisional reorientations, spin evolution, and gravitational resonances. In practice, the transport from the whole main belt → NEO is characterized by a size-dependent mean decay time scale τ_{mb}. The time scale of main belt bodies must be relatively long, otherwise the NEO population is 'overshoot' (see Fig. 3). On the other hand, the transport from the NEO → trash bin is very short (8 My), which is comparable to Granvik et al. (2018) (6 to 11 My; see their Fig. 15).

The nominal time span of our simulations is 4.4 Gy, to leave some space for the early evolution, without solving a question, whether the evolution was very early or not (cf. Brož et al. 2021). Of course, cratering may be also produced very early, but hereinafter we assume a completeness and no crater erasure for simplicity. Consequently, we should never 'overshoot' the observed record.

Our modelling certainly has some caveats. For example, it is not certain whether the initial SFD of the early main belt should be broken at 20 km, or at 15 km; the initial slope q in the size range $D \in (10; 100)$ km could be possibly steeper; the average density **could** be $2\,\mathrm{g\,cm^{-3}}$ instead of $3\,\mathrm{g\,cm^{-3}}$; possibly, there are two or even more rheologies for S- and C-type populations; the YORP spin-up may destroy bodies instead of affecting transport; etc.

4. Extrapolated size distributions

For each of the families, the collisional model must be set up individually. The initial conditions correspond to the age of the family, which is unknown. Consequently, both the main belt and the family SFDs must be adapted, so that the final conditions correspond to the observations. The SFD was characterized by the largest remnant (LR), the largest fragment (LF), and the power-law cumulative slopes: q_{a}, q_{b}, q_{c}, q_{d}, with the diameter ranges specified by: D_1, D_2, D_3. Again, every model was run at least 10 times to determine its uncertainties, which are mostly due to stochasticity of collisions, or break-ups of large asteroids with a fractional probability. We always tried to use the simplest initial conditions possible, i.e., a simple power law $q_{\mathrm{a}} = q_{\mathrm{b}}$, which subsequently 'breaks' in the course of collisional evolution, $q_{\mathrm{a}} > q_{\mathrm{b}}$. The values of q_{c} or q_{d} must be less steep than −3 to prevent a divergence of mass. If it did not work, because the initial conditions were not simple, we prepared a more complicated model(s). Generally speaking, the use of collisional evolution to constrain the age of asteroid families dates back to the work of Marzari et al. (1995). Here we profit from having information about SFD to significantly smaller size than three decades ago.

Our results for relatively young families, (Merxia, Agnia, Juno), as well as some old families (Vesta, Koronis, Flora), suggest the possibility that their SFDs were initially simple power-laws, starting at the largest fragment and ending even below the observational incompleteness (see Fig. 5). Ages of these families are easy to estimate (see Table 2). We wait until the SFD 'breaks' to two power-laws and fits the observed SFD. The break is induced by main belt ↔ family or secondary collisions and is typically at $D \doteq 5$ km.

However, remaining families required more complicated initial conditions (Massalia, Maria, Gefion, Eunomia), as demonstrated in Fig. 5. It may also indicate a different age, or a mismatch between collisional and orbital models. The ages derived from orbital models are discussed in Appendix B.

Technical intermezzo. Maria's SFD often 'undershoots' the observed one at $D \simeq 1$ km which would correspond to less than 2500 My (not to 3000 My as suggested by orbital models); it is also very shallow at large sizes, which is typical for interlopers.

Gefion's SFD often 'overshoots' for the age 470 My (Nesvorný et al. 2009) and the only way how to fit it is again a broken power-law. On the other hand, if the initial SFD is a simple power-law $q_{\mathrm{a}} = q_{\mathrm{b}} = -4.6$, the best-fit is obtained natu-

Table 2. Ages of the S-type families estimated from our collisional model.

family	age
–	My
Vesta (HED)	1100 ± 100
Phocaea (H)	700 ± 100
Maria (H)	2500 ± 300
Merxia (H)	330 ± 50
Agnia (H)	100 ± 50
Koronis (L/H)	2200 ± 300
Massalia (L)	800 ± 100
Gefion (L)	1500 ± 200
Juno (L/LL)	750 ± 100
Flora (LL)	1200 ± 200
Eunomia (LL)	4200 ± 300

rally for 1500 My which might be more compatible with Aljbaae et al. (2019).

In the case of Massalia, a broken power-law must be used to obtain a fit at 150 My. For a simple power-law with the cumulative slopes $q_a = q_b = -7.5$, the age would be as long as 800 My.

Eunomia's SFD at $D \simeq 20$ km is wavy, which is either related to the primordial SFD, or interlopers. Its SFD at multi-km sizes is very shallow, actually the most shallow of all families, which indicates a significant depletion of objects and a preference for an older age (definitely more than 3000 My).

Taken overall, ages seem to be self-consistent; none is older than 4.4 Gy and they are distributed over the whole interval 0 to 4.4 Gy.

Main belt population at 1 metre. For metre-sized bodies, there is inevitably some stochasticity, about half-order in the absolute number of bodies, due to secondary collisions and temporally variable tail. Consequently, for H-chondrite families, the populations are (in 10^{10} units):

Karin (30-60) → **Koronis** (2-4) → Maria (0.8-2) → Agnia (1-2) → Phocaea (0.5-1) → Merxia (0.3-0.9);

for L-chondrite:

Karin (30-60) → **Koronis** (2-4) → **Juno** (0.5-1.5) → Gefion (0.5-1.5) → Massalia (0.4-1);

for LL-chondrite:

Eunomia (1-6) → Flora (2-4) → **Juno** (0.5-1.5).

For Karin, see again Sec. 8 . Otherwise, the order is similar for metre- and kilometre-sized bodies. Maria is similar to Agnia within stochasticity; Juno to Gefion **or Massalia**; Eunomia might be slightly more populous than Flora. Let us recall all these populations are still in the main belt; a transport is yet to be applied.

5. NEO population at 1 kilometre

We used our orbital model described in Brož et al. (2011) to determine the decay time scales in the main belt and the life times among the NEOs. It is based on the symplectic integrator SWIFT-RMVS3 (Levison & Duncan 1994). The dynamical model includes: 11 mutually interacting bodies (Sun, Mercury to Neptune, Ceres, Vesta), the Yarkovsky effect (Vokrouhlický 1998; Vokrouhlický & Farinella 1999), the YORP effect (Čapek & Vokrouhlický 2004), collisional reorientations, a mass shedding, and the strength-dependent spin limit (Holsapple 2007).

Table 3. Parameters of the synthetic families used in our orbital models.

family	v_5	D_5	α	f	ω
–	m s^{-1}	km		deg	deg
Vesta (HED)	200	2	−0.5	90	120
Phocaea (H)	30	5	−0.5	30	0
Maria (H)	50	5	−0.5	90	90
Merxia (H)	24	5	−0.5	90	90
Agnia (H)	15	5	−0.5	30	0
Koronis (L/H)	50	5	−0.5	30	30
Karin (L/H)	5	5	−0.5	30	0
Massalia (L)	24	5	−1.0	90	130
Gefion (L)	100	2	−0.5	90	30
Juno (L/LL)	100	2	−0.5	90	30
Flora (LL)	100	2	−0.5	90	90
Eunomia (LL)	100?	2?	0.0	90	50

Notes. v_5 denotes the ejection velocity, D_5 the reference size, α the exponent of the distribution, f the true anomaly, ω the argument of pericentre.

This is supplemented by a series of digital filters to compute mean elements (Quinn et al. 1991) and proper elements (Šidlichovský & Nesvorný 1996).

Some of the parameters were common for all simulations. Namely, a time step $\Delta t = 9.13125$ d, output of osculating elements 10 ky, sampling of osculating elements 1 y, sequence of filters A, A, A, B, decimation factors 10, 10, 10, 3, output of mean elements 3000 y, number of samples for the Fourier transform 1024, output of proper elements 0.1 My, a thermal capacity $C = 680\,\mathrm{J\,kg^{-1}\,K^{-1}}$, thermal conductivity $K = 10^{-3}\,\mathrm{W\,m^{-1}\,K^{-1}}$, thermal emissivity $\epsilon = 0.9$, Bond albedo $A = 0.1$, surface density $\rho = 1.5\,\mathrm{g\,cm^{-3}}$, YORP efficiency $c_{\mathrm{YORP}} = 0.33$, reorientation time scale $B = 84.5$ ky, with exponents $\beta_1 = 0.83$, $\beta_2 = 1.33$, and normalisations $\omega_0 = 3.49 \times 10^{-4}\,\mathrm{rad\,s^{-1}}$, $D_0 = 2.0$ m, cohesive strength scale $\kappa = 2.27{\times}10^7\,\mathrm{g\,cm^{-1/2}\,s^{-2}}$, friction coefficient $s = 0.25$, relative axial ratios $c/a = 0.7$, $b/a = 0.7$, ...

Others were specific, adapted for individual families. We always tried to create an initial synthetic family in such a way, that will –after the long-term evolution– end up as similar to the observed family (see, e.g., Brož & Morbidelli 2013). Parameters of the principal bodies ('parent bodies') are discussed in Appendix A. Probably the most important choice is the initial velocity field. According to the rule: 'either escape or not escape', we created a distribution with the peak at about the escape speed v_{esc} from the respective parent body. For simplicity, we assumed an isotropic field. (Even a cratering is approximately isotropic in shifted coordinates.) Moreover, we assumed a size-dependent relation (Vokrouhlický et al. 2006b):

$$v(D) = v_5 \left(\frac{D}{D_5} \right)^{\alpha} . \tag{4}$$

The geometry in the $(a, e, \sin I)$ space is further determined by the true anomaly f and the argument of pericentre ω. Sometimes, these are still visible in the observed distribution of elements. This is true not only for Karin, but also for much older families (Brož & Morbidelli 2013; Marsset et al. 2020). These parameters are listed in Tab. 3

The results of our simulations are summarized in Fig. 7, Fig. 8, and the respective time scales are listed in Table 4.

Steady-state situation. To estimate the number of 1-km bodies in the NEO population, we can assume a steady state. In this situation:

$$N_{\rm neo}(>1\,{\rm km}\,|\,{\rm H}) = \int_0^\infty C N_{\rm mb}(>1\,{\rm km})\,p({\rm H})\,\frac{f(\tau_{\rm neo})\tau_{\rm neo}{\rm d}\tau_{\rm neo}}{\tau_{\rm mb}}\,, \quad (5)$$

where C denotes the calibration, p the probability that the family contributes to H, $\tau_{\rm neo}$ the life time in the NEO population, f the corresponding distribution function, and $\tau_{\rm mb}$ the life time in the main belt population; and similarly for 1-m size and similarly for L, LL. For constant factors, Eq. (5) simplifies to:

$$N_{\rm neo}(>1\,{\rm km}\,|\,{\rm H}) = C N_{\rm mb}(>1\,{\rm km})\,p({\rm H})\,\frac{\bar\tau_{\rm neo}}{\tau_{\rm mb}}\,, \quad (6)$$

where $\bar\tau_{\rm neo}$ denotes the mean lifetime in the NEO population. Actually, this is the very reason why the median must *not* be used. However, short-lived NEO orbits are common and long-lived ones are exceptional (see Fig. 8). In other words — outliers determine the mean value. One solution is to use a as many orbits as possible (or orbital clones). However, the total number of bodies entering the NEO region is limited, because we study individual families. In other words — a poor sampling of τ's (hence low $\bar\tau$) may be more realistic than fine sampling (high $\bar\tau$).

Moreover, the NEO orbits sometimes require a very fine time step (0.25 d), if the eccentricity is extreme (Granvik et al. 2018); this problem is especially urgent for the ν_6 resonance, which pushes $e \to 1$. For some families (Vesta, Flora) we thus used $\tau_{\rm g18}$ from Tab. 4.

Today, the Flora family seems to provide a dominant contribution to the population of kilometre-sized NEOs, followed by Vesta, Juno, Eunomia. This approximately corresponds to the percentages of observed NEOs. However, we should take into account also the background population which is substantial. It is probably not surprising, because the 11 families discussed in this work contain just 57.1×10^3 of 1-km bodies out of 1360×10^3 present in the main belt, i.e., less than one twentieth. One possible interpretation is that the background population is indeed spectrally similar to the families.

Non-stationary situation. If we relax the assumption above, we have to compute the dynamical decay and transport from the main belt → NEO as non-stationary:

$$\dot N_i = -\frac{1}{\tau_i}N_i\,, \quad (7)$$

$$\dot N_j = +\frac{1}{\tau_i}N_i - \frac{1}{\tau_j}N_j\,, \quad (8)$$

where the index $i = 1..M$ corresponds to the families, $j = 1..M$ to the NEO populations, respectively. If $\dot N_j = 0$ is assumed, Eq. (8) simplifies to Eq. (6), provided τ_j is represented using $\bar\tau_{\rm neo}$ (i.e., main-belt population $N_{\rm mb}$ decay over the $\bar\tau_{\rm neo}$ timescale neglected).

To demonstrate, how contributions change in the course of time, due to dynamical decay alone, we solved the set of Eqs. (7) and (8), and plotted the solution in Fig. 11. Of course, a collisional decay occurs at the same time; it should be solved self-consistently by a collisional model. Nevertheless, Fig. 11 suggests that family contributions to the NEO population in the past must have been variable. It may also suggest a lower collisional activity between approximately 4 and 2.5 Gy ago, but it sensitively depends on individual ages of families (cf. Sec. 9.2).

Given the overall decay of individual families (both collisional and orbital), they can hardly be in a steady state! If true, Eq. (6) is questionable, as is the very method for estimation of the NEO population, because we do not know the derivatives $\dot N_j$'s. In principle, we can use the observations to determine N_j's and compute $\dot N_j$'s, but not the other way round.

6. NEO population at 1 metre

The evolution of metre-sized bodies was computed in the same way. Their initial conditions were modified though — we used the current orbits of family members, because these fragments are continuously replenished by collisions. The time span is relatively short, 50 My, which is sufficient to measure the decay time scale. Our results are summarised in Fig. 9, Fig. 10, and in Tab. 5.

The situation is more complex for metre-sized bodies. There are inevitable uncertainties stemming from a variable 'tail' of the SFDs. HED and LL-chondrite-like families contribute comparably (Vesta 4.3-15.2 × 10^8, Flora 6.3-12.5 × 10^8), in agreement with the observations. If the absolute number of *all* metre-sized NEOs is **200-300** $\times10^8$ **(Harris & Chodas 2021)**, and the percentages of meteorite classes HED 6.2 %, LL 8.2 %, one would expect **12.4-18.6** $\times10^8$, **16.4-24.6** $\times10^8$, respectively. This is not far from our synthetic numbers, given the fact that scattered V-types (not associated with Vesta) also contribute to HED and that other families (Eunomia, Juno) also contribute to LL. **For simplicity, we assumed that percentages of meteorites correspond to the percentages of meteoroids, even though: the flux is dependent on collisional probabilities (cf. Tab. D.3); some meteoroids might be more fragile (e.g., carbonanceous chondrites), and disintegrate during their atmospheric entry, which would decrease the absolute numbers above.**

On **the** contrary, H- and L-chondrite-like bodies are underestimated compared to the observations**.** If the percentages are H 33.8 %, L 37.0 %, one would expect up to **67-101** $\times10^8$, **74-111** $\times10^8$ bodies. This is different by a factor of more than ∼10. While this is a serious mismatch ('conundrum'), it is a confirmation that background or other families, possibly much younger, should be taken more seriously.

Table 4. Dynamical time scales and cumulative numbers of 1-km asteroids in the main belt (mb) and the near-Earth region (neo).

family	res.	τ_{g18}	1-km τ_{neo}	1-km τ_{mb}	ρ	1-km N_{mb}	1-km N_{neo}	obs.	obs.
–	–	My	My	My	g cm^{-3}	10^3	1	1	%
Vesta (HED)	ν_6	6.98	0.57[6]	3313	2.5!	11.4	24.0	24	8
Phocaea (H)	ν_6	6.98	5.91	796	2.5	2.7	20.0!	6	2
Maria (H)	3:1	1.83	0.95[4]	1524	3.0	5.5	3.4	17	5
Merxia (H)	5:2	0.68	0.22	596	2.5	2.0	0.7	12	4
Agnia (H)	5:2	0.68	0.19	1004	2.5	3.1	0.6	12	4
Koronis (L/H)	5:2	0.68	0.81[4]	1404	3.0	9.2	5.3	12	4
Karin (L/H)	5:2	0.68	0.22[u]	921[a]	2.5	1.1	0.3	–	–
Massalia (L)	3:1	1.83	0.45	1018	2.5!	2.6	1.1	16	5
Gefion (L)	5:2	0.68	0.69	760	2.5!	3.8	3.5	11	4
Juno (L/LL)	8:3	1.70	2.49	627	2.5	4.2	16.6	29	9
Flora (LL)	ν_6	6.98	0.37[6]	669	2.5	7.2	**75.1**	**158**	51
Eunomia (LL)	3:1	1.83	4.48	3335	3.54	7.0	9.4	14	5
HED							24.0	24	8
H							31.7	59	19
L							21.3	56	18
LL							84.5	172	55
H+L+LL						48.4!	137!	287?	91
all S-types						231?		287?	
all bodies						1360		925	

Notes. For all families, we report the neighbouring resonances, the NEO life time τ_{g18} from Granvik et al. (2018), the NEO life times τ_{neo} from this work, computed for 1-km bodies, the main belt life times τ_{mb}, the volumetric density of simulated bodies, the observed cumulative number $N_{mb}(>1\,\mathrm{km})$ of main belt bodies, the computed cumulative number N_{neo} of NEOs and meteoroids, along with the observed N_{neo} from **this work**, where the original percentages were multiplied by the total number of S-type NEOs ($925 \times 31\,\% \doteq 287$; Marsset et al. 2022). For comparison, the fraction of S-type main belt bodies is different ($1360 \times 10^3 \times 17\,\% \doteq 231 \times 10^3$; Gradie et al. 1989). Additional notes: [4] 4 outer planets; [u] undersampled; [a] after 100 My; [6] problem with the ν_6 resonance (τ_{g18} is used instead of τ_{neo}).

Table 5. Same as Tab. 4 for 1-m meteoroids.

family	res.	τ_{g18}	1-m τ_{neo}	1-m τ_{mb}	ρ	1-m N_{mb}	1-m N_{neo}	obs.	obs.
–	–	My	My	My	g cm^{-3}	10^{10}	10^8	10^8	%
Vesta (HED)	ν_6	6.98	2.50	115	2.5!	2-7	4.3-15.2!		6
Phocaea (H)	ν_6	6.98	7.24	114	2.5	0.5-1	3.2-6.4!		2
Maria (H)	3:1	1.83	1.82	98	2.5	0.8-2	1.5-3.7		15
Merxia (H)	5:2	0.68	0.43	81	2.5	0.3-0.9	0.2-0.5		7
Agnia (H)	5:2	0.68	0.34	103	2.5	1-2	0.3-0.7		8
Koronis (L/H)	5:2	0.68	0.26	201	2.5	2-4	0.3-0.5		8
Karin (L/H)	5:2	0.68	0.27	149	2.5	30-60	3.9-7.8!		–
Massalia (L)	3:1	1.83	3.83	139	2.5!	0.4-1	1.1-2.8		17
Gefion (L)	5:2	0.68	0.32	75	2.5!	0.5-1.5	0.2-0.6		6
Juno (L/LL)	8:3	1.70	1.38	204	2.5	0.5-1.5	0.3-1.0!		**23**
Flora (LL)	ν_6	6.98	3.45	110	2.5	2-4	**6.3-12.5**		7
Eunomia (LL)	3:1	1.83	1.56	199	2.5!	1-6	0.8-4.7!		1
HED							4.3-15.2	10-15	6
H							9.4-19.6!	67-100	40
L							1.6-4.4!	77-116	46
LL							7.1-17.2	13-20	8
H+L+LL						39.0-83.9	18.1-41.2	158-237?	94
all S-types								158-237?	
all bodies						400-1200	400-800	**200-300**^{H}	
with 2nd Koronis:									
Koronis$_{(2)}$	5:2	0.68	0.26	201	2.5	~100-300?	12.9-38.8		–
H							22.3-58.4	67-100	40
with 2nd Massalia:									
Massalia$_{(2)}$	3:1	1.83	3.83	139	2.5!	~10-30?	27.6-82.7		–
L							29.2-87.1	77-116	46

Notes. The observed *percentages* of meteorites **from this work.** For comparison, the observed percentages of meteorite falls from `https://www.lpi.usra.edu/meteor/`, `https://metbase.org/` with respect to *all* classes are: HED 6.2 %, H 33.8 %, L 37.0 %, LL 8.2 %, respectively. Additional notes: ^{H} Harris & Chodas (2021).

7. Meteorite–NEO conundrum

A main result from our simulations is that large asteroid families, when taken together, do not allow solving the meteorite–NEO conundrum. It is quite the opposite, they perfectly illustrate the conundrum. Whereas these families are plausible sources for a large fraction of the $D \geq 1$ km NEO population (Sect. 5), they cannot be the source of the vast majority of meteorites and **meteoroids** delivered to Earth today **(Sect. 6)**.

To illustrate this more clearly, **we** consider Vesta and its family as **an** instrument of logic and ground truth. There are **almost none** V-types outside of the Vesta family. Our calculations for 1-m NEOs (Tab. 5), and considering large families only, indicate that for 1 HED we should recover 2 OCs. Yet meteorite fall statistics are closer to 1 HED for 13 OCs. Following our simulations, the only way to reach a reasonable HED/OC ratio is to consider the whole belt as the source of OCs (Tab. 5), with relatively fair/equilibrated contributions from the inner, middle and **possibly also** outer **belt.**

Meteorite measurements including fresh fallen as well as fossil meteorites, however, indicate that a fair contribution of all S-type main belt asteroids to the OC flux is naïve and essentially wrong. Instead, recent asteroid breakup events (≤ 500 My) are likely the ones influencing most contemporary meteorite fall statistics. This is well illustrated by the distribution of the cosmic ray exposure (CRE) ages (Marti & Graf 1992; Graf & Marti 1994, 1995) and ^{40}Ar/^{39}Ar impact ages (Swindle et al. 2014 and references therein) of OCs. Notably, about **30%** of all H chondrites have CRE ages in the **5**-8 My range indicating **one or more recent breakups** of H-like S-type **asteroids**.

Regarding L chondrites, 40-50% of them are heavily-shocked (e.g., Graf & Marti 1995; Rubin 1994; Bischoff et al. 2019 and references therein) and degassed with ^{40}Ar/^{39}Ar ages near 470 My (e.g., Korochantseva et al. 2007; Swindle et al. 2014) suggesting that an L chondrite-like asteroid suffered a major impact ~ 470 My ago (Haack et al. 1996) and that this impact is still at the origin of 15-20% of all meteorite falls today. Studies of fossil meteorites found in a ~ 467 My old Ordovician strata in a limestone quarry in Sweden (Schmitz et al. 1997, 2001) support these findings and further revealed that the measured abundance of fossil L chondrites implies a rate of meteoritic bombardment 1 to 3 orders of magnitude higher than at present (Heck et al. 2017; Terfelt & Schmitz 2021)), with L chondrites representing $\geq 99\%$ of all falls just after the impact. To illustrate the sudden change in meteorite fall statistics induced by **a** large **collisional** event in the main belt, Heck et al. (2017) recovered **relic** minerals from coarse micrometeorites in a limestone that formed about one million years before the breakup of the L-chondrite parent **body** and showed that achondrites had similar or **even** higher abundances than **OCs**.

In summary, both our simulations and meteorite measurement support the idea that asteroid families older than 1 Gy, even if prominent **according to** the number of $D \geq 1$ km family members, are modest contributors to the current meteorite flux. Nonetheless, these older families may host new families that may be at the origin of a meteorite flux increase, such as the young Karin family located in the **old** Koronis family.

8. The Karin collisional series

As an example of a possible contribution of **young** families, we studied the Karin family = FIN 610, i.e., a secondary breakup in the Koronis family (L/H) with the age 5.8 My (Nesvorný & Bottke 2004; Carruba et al. 2016). It contains 1.1×10^3 of kilometre-sized bodies and up to 30 to 100×10^{10} of metre-sized bodies. It is clearly a non-steady population.

Contrary to our expectations, the Karin family may contribute more than any other family to the population of metre-sized bodies if its initial SFD was a power-law with the cumulative slope −2.9 down to 1 m. Indeed, the observed SFD is a *perfect* power-law down to the observational completeness (Fig. 12) and the 'tail' of the SFD simply had not have enough time to evolve; it takes 30 My to decrease below Koronis (Fig. 13).

An important question is: is there enough time to deliver bodies to the NEO space? Yes and no. The expected Yarkovsky drift rate (without YORP) is up to 0.0003 or 0.06 au My^{-1}, for 1-km or 1-m bodies, respectively. The distance to the neighbouring resonance 5:2 is 0.03 to 0.05 au. Consequently, it would take about 100 My, until kilometre-sized bodies are delivered, but only a few My for metre-sized bodies, depending on their spin axis orientations.

Alternatively, one can assume that metre-sized fragments were ejected at significantly larger speeds, as in Eq. (4). This would make even an early transport possible. It is closely related to an equipartition of kinetic energy between high-mass and low-mass fragments, as seen in some SPH simulations of break-ups (Vokrouhlický et al. 2021). Nevertheless, most fragments colliding with the Earth today must have been travelling in space for approximately 5.8 My.

Moreover, according to our analysis, there is not a single family, but four. The second one is Koronis$_{(2)}$ = FIN 621 (Molnar & Haegert 2009), or a cratering event on Koronis itself. Its SFD is even steeper (−4.0; Fig. 12), so that it **likely dominates** Karin **already** for $D \lesssim 0.5$ km. We discovered the third and the fourth family when looking at $a_\mathrm{p}, e_\mathrm{p}, \sin I_\mathrm{p}$ from a suitable direction. The concentration or correlation of orbits is shown in Fig. 14. They are logically more dispersed, as small fragments have already reached the resonances (5:2, 17:7). It is a confirmation that such collisions are still ongoing within the parent family (i.e., Koronis$_{(1)}$).

In other families, like Eunomia, these sub-clusters are not seen, which is an argument in favour of the collisional cascade being driven by secondary collisions. However, we should estimate it explicitly (in the same way as in our collisional model). A projectile of diameter d is needed to disrupt a target of diameter D:

$$d = D\left(\frac{2Q}{v^2}\right)^{\frac{1}{3}}, \tag{9}$$

where Q is the specific energy and v the projectile speed. The frequency of collisions (in y^{-1}) is:

$$f = p\frac{D^2}{4} f_\mathrm{g} N(>D)\, N(>d), \tag{10}$$

where p denotes the intrinsic collisional probability (in km^{-2} y^{-1}; Tab. D.1), f_g the gravitational focussing factor, and N's the respective numbers of available targets and projectiles. For main belt–main belt collisions, $D = 30$ km, $Q = Q^\star$ (i.e., catastrophic disruptions), $d = 3.9$ km, $N(>D) = 1330$, $N(>d) = 129000$, we obtain $f = 1.1 \times 10^{-7}$ y^{-1}, or $1/f = 9$ My Consequently, it is not surprising that we observe a Karin-like event.

On the other hand, Koronis–Koronis collisions occur with much higher probabilities (Tab. D.1), lower impact speeds, much lower numbers of bodies; $d = 9.1$ km, $N(>D) = 10$, $N(>d) = 145$, hence $f = 4.3 \times 10^{-12}$ y^{-1}. What we see in Koronis, is not

a cascade of secondary collisions, but rather a series of primary collisions.

There might still be some caveats in our estimates: (i) the Karin and Koronis$_{(2)}$ families had similar nodes and similar precession rates, while p's were computed for a uniform distribution of nodes; (ii) even cratering events ($Q \ll Q^\star$) are capable of producing numerous fragments; (iii) a population of sub-km asteroids may have a different spatial distribution as well as p's with respect to Koronis; (iv) a production of S-type metre-sized fragments might have been temporarily increased by another collisions (e.g., with C-type fragments from the Veritas family; Farley et al. 2006).

Nevertheless, if Karin-like events remain observable for at least **50** My, we predict there should be more than **5** of them. Moreover, if such events produce steep SFD's, as suggested by Fig. 12, they **certainly** dominate Koronis-like families at sub-km sizes as well as at metre sizes via a collisional cascade.

9. Discussion

9.1. IRAS dust bands

The Karin family event produced also dust, which was observed by the IRAS as **the** 2.1° band of infrared radiation (Sykes 1990; Reach et al. 1997; Nesvorný et al. 2006), i.e., at exactly the same inclination as the family. The equivalent diameter of all dust particles is approximately $D \simeq 11$ km (Nesvorný et al. 2006, cf. Tab. 6). **According to the Long Duration Exposure Facility (LDEF; Love & Brownlee 1993), the dominant size of dust particles is** $d = 100\,\mu$m**,** which corresponds to the number of particles $N(>100\,\mu\text{m}) = 1.3 \times 10^{24}$.

Our extrapolated SFD of the Karin family, with the slope −2.9 determined for multi-kilometre asteroids, predicts the number of particles $N(>100\,\mu\text{m}) = 2.7 \times 10^{23}$, which is surprisingly close to the IRAS value (see Fig. 15). In other words, our SFD seems to be reliable over **8** orders of magnitude.

The factor of ∼5 difference indicates that the SFD slope is (was) even steeper, possibly close to −3.0. This is a special value, because it corresponds to a log-uniform distribution in mass. In math, it results from a reciprocal of a uniform random variable, $\frac{1}{x}$. In our case, every order of magnitude in size (10 km–1 km, 1 km–100 m, ... 1 mm–100 μm) contains about the same amount of mass. **The equivalent diameter of all orders is only** $8^{1/3} = 2$ **times larger.** It is *not* divergent in mass, simply because we do not continue to 0.

For Koronis$_{(2)}$, a straight extrapolation to 100 μm **is impossible, because its slope is too steep** (−4.0)**; it cannot be kept due to very frequent collisions. If extrapolate the SFD just by one order of magnitude to 0.1 km, and assume a collisional equilibrium with the main belt** (−2.7)**, it turns out that Koronis$_{(2)}$ also contributes to the** 2.1° **dust band, but it can be hardly distinguished from Karin.**

Interestingly, the inclination of (20) Massalia corresponds exactly to one of the dust bands, namely at 1.4° **(Nesvorný et al. 2006, Fig. E.1). This association is much more likely than with (656) Beagle (Nesvorný et al. 2008), because the temperature profile, constrained by IRAS 12-, 24- and 60-**μm **band observations, indicates hotter dust grains. If true, the Massalia family (or its part) is younger than previously thought. Again, its slope** −2.8 **seems to be in agreement with the dust population,** $N(>100\,\mu\text{m}) \simeq 4 \times 10^{23}$ **(Fig. 16).**

Table 6. Possible correspondence of dust bands and family-formation events.

band	D	family
–	km	–
1.4°	4	Massalia$_{(2)}$ (L)
2.1°	11	Karin series (L/H)
9.8°	14	Veritas (C)
all	23	zodiacal cloud

Notes. D denotes the equivalent diameter of all dust particles from Nesvorný et al. (2006).

Table 7. Possible correspondence of shock ages of **OCs** and family-formation events.

shock	family	
My	–	
100	Agnia (H)	
400	Merxia (H)	
900	**Phocaea (H)**	
3600	Maria (H)	if older
3900	Koronis (L/H)	if older
470	Gefion (L)	if younger
470	Juno (L/LL)	
470	**Massalia (L)**	if younger
500?	Juno (L/LL)	
1000?	Flora (LL)	
4200	Eunomia (LL)	

9.2. Radiometric shock ages

OCs have measured shock ages, and their distribution exhibits 'peaks' (Swindle et al. 2014). Sometimes, they might be related to very precise measurements, but at least some of them are real peaks. Do they correspond 1:1 to family-formation events? A 'nihilistic' answer would be no; or not necessarily. Nevertheless, for the moment, let us assume yes.

A possible correspondence is summarized in Tab. 7. All groups include numerous shock ages around 4560 My, most likely related to accretion. For H-chondrite families, there are logical candidates for relatively young shock ages. Old shock ages might be related to Maria, Koronis, if these families are about 50 % older. This is indeed possible if the initial SFDs were about 50 % more populous.

For L-chondrite shock age 470 My, there is a known candidate the Gefion family (Nesvorný et al. 2009), but its SFD indicates much older age (cf. Tab. B). A viable alternative might be the Juno family (of L/LL type), **or the Massalia family.** Note: (3) Juno is the 2nd largest S-type asteroid.

For LL-chondrite, there are two minor peaks, possibly related to Juno or Flora. On the other hand, the major peak at 4200 My might be related to Eunomia. Note: (15) Eunomia is the 1st largest S-type asteroid.

Unfortunately, the sample of Swindle et al. (2014) is still limited. Ideally, one should have multiple meteorites with the same shock age, or more importantly, statistically significant 'gaps' in between, similar to the one between 1500 and 3500 My for H chondrites. Moreover, one cannot exclude a possibility that shocks originated in secondary collisional cascade, minor cratering events, microimpacts, etc.

Table 8. Possible correspondence of cosmic-ray exposure ages of **OCs** and recent family-formation events.

exposure My	family –
6	Karin (L/H)
8	Koronis$_{(2)}$ (L/H)?
20?	Karin series (L/H)?
30?	Karin series (L/H)?
40?	**Massalia**$_{(2)}$ (L)?
15?	? (LL)

9.3. Radiometric cosmic-ray exposure ages

Similarly, **OCs** have measured cosmic-ray exposure ages (Eugster et al. 2006), which are unevenly distributed. A possible correspondence with recent family-formation events is summarized in Tab. 8. It is not **very** conclusive, because the only candidate for the **prominent** H-chondrite peak between 6-8 My is the Karin family, and for the **remaining distribution** the Karin series**.**

Unfortunately, the L-, LL-chondrites peaks are much less prominent and the distributions seem to be broad. The range from 10 to 40 My is characteristic for collisional or transport time scales of metre-sized bodies. According to the dust bands (Sect. 9.1), the only possibility seems to be the young Massalia family, which age should coincide with the upper limit.

10. Conclusions

In this work, we evaluated the contribution of major S-type asteroid families to the NEO and meteoroid populations. We used **up-to-date catalogues** to constrain the main belt populations of kilometre-sized bodies and extrapolated them down to metre-sized bodies, using a calibrated collisional model. For all families, we also modelled transport from the main belt, to obtain the respective time scales and life times among NEOs.

The SFDs are constrained very well at a 1-km size. **The resulting numbers of kilometre-sized NEOs from our model seem to be in agreement with the MITHNEOS survey (Marsset et al. 2022; Marsset & et al. submit.); including the spectroscopic classification of NEOs to HED, H, L, and LL types (Tab. 5). Our analysis allowed us to address important questions.**

Why Flora (LL) contributes so much to NEOs? Eunomia and Flora have similar SFDs**,** but the ratio of time scales $\tau_{\rm mb}$ times the ratio of life times $\tau_{\rm neo}$ is unfavourable for Eunomia.

Why Juno (L/LL) contributes so much to NEOs? It has a steeper SFD than Gefion, **and the ratio of life times $\tau_{\rm neo}$ is favourable for Juno.**

Why several H-type families contribute to NEOs? Because their populations are comparable to each other, and their dynamics is not so different from each other. It demonstrates the importance of using a number of sources in the model, otherwise, it is impossible to decide which source is important (cf. Phocaea, Koronis, Maria, . . .).

On the other hand, the extrapolation **of SFDs** to a 1-m size is more uncertain. **While we** can **explain** the absolute numbers of **HED and LL** metre-sized meteoroids, because they likely originate from the **corresponding** families **(i.e., Flora and Vesta)**, **we are unable to explain** H and L meteoroids **this way**. **The statistics of corresponding meteorites is** approximately H/L ~ 1, LL/HED ~ 1, but H/LL ~ 4. **Because our model systematically indicates H/LL ~ 1, we conclude that H and L meteorites must originate from other sources (cf. Tab. 5).**

This is likely related to a more general problem of the modelling. A steady state was **assumed** to compute the **meteoroid** populations, but **young families** contributions may be non-stationary. **Their SFDs may be temporarily steep at sub-km sizes. In fact, the meteorite flux has not been always constant, neither recently (Drouard et al. 2019), nor long time ago (Heck et al. 2017). This points to more recent or transient sources of metre-sized bodies.**

In this context, we reported a discovery of the Karin collisional series, **composed of four sub-families. Its SFD is steep and its extrapolation ('tail') down to 100-μm sizes is confirmed by the IRAS** 2.1° **dust band (Nesvorný et al. 2006). Moreover, its interpolation to 1 m shows that Karin, together with other sub-families, in particular Koronis$_{(2)}$, should dominate the population of H meteoroids (see Tab. 5, Fig. 15). This is the most straightforward explanation of the NEO–meteorite conundrum.**

Using analogous arguments, the Massalia family (or its part) should dominate the population of L meteoroids (Tab. 5, Fig. 16). This family is conveniently located in the inner belt, and has exactly the same inclination as the IRAS 1.4° **dust band. In order to explain the distribution of radiometric ages (Eugster et al. 2006; Swindle et al. 2014), we predict that the family is composed of old and young parts, with overlapping velocity fields, because both collisions occurred on the same body (i.e., (20) Massalia).**

Acknowledgements. This work has been supported by the Czech Science Foundation through grant 21-11058S (M. Brož and D. Vokrouhlický). We thank B. Bottke for sharing his program for computations of collisional probabilities with us. We thank M. Granvik for discussions about the subject of this work.

References

Aljbaae, S., Souchay, J., Prado, A. F. B. A., & Chanut, T. G. G. 2019, A&A, 622, A39
Benz, W. & Asphaug, E. 1999, Icarus, 142, 5
Bischoff, A., Schleiting, M., & Patzek, M. 2019, Met. Planet. Sci., 54, 2189
Bottke, W. F., Brož, M., O'Brien, D. P., et al. 2015, The Collisional Evolution of the Main Asteroid Belt, 701–724
Bottke, W. F., Durda, D. D., Nesvorný, D., et al. 2005, Icarus, 179, 63
Bottke, W. F., Morbidelli, A., Jedicke, R., et al. 2002, Icarus, 156, 399
Bottke, W. F., Vokrouhlický, D., Ballouz, R. L., et al. 2020, AJ, 160, 14
Brož, M. & Morbidelli, A. 2013, Icarus, 223, 844
Brož, M., Vokrouhlický, D., Morbidelli, A., Nesvorný, D., & Bottke, W. F. 2011, MNRAS, 414, 2716
Brož, M., Chrenko, O., Nesvorný, D., & Dauphas, N. 2021, Nature Astronomy, 5, 898
Brož, M., Morbidelli, A., Bottke, W. F., et al. 2013, A&A, 551, A117
Čapek, D. & Vokrouhlický, D. 2004, Icarus, 172, 526
Carruba, V. 2009, MNRAS, 398, 1512
Carruba, V. & Nesvorný, D. 2016, MNRAS, 457, 1332
Carruba, V., Nesvorný, D., & Vokrouhlický, D. 2016, AJ, 151, 164
Carry, B. 2012, Planet. Space Sci., 73, 98
Ceplecha, Z. 1992, A&A, 263, 361
de León, J., Licandro, J., Serra-Ricart, M., Pinilla-Alonso, N., & Campins, H. 2010, A&A, 517, A23
Drouard, A., Gattacceca, J., Hutzler, A., et al. 2019, Geology, 47, 673
Dunn, T. L., Burbine, T. H., Bottke, W. F., & Clark, J. P. 2013, Icarus, 222, 273
Durda, D. D., Bottke, W. F., Nesvorný, D., et al. 2007, Icarus, 186, 498
Eugster, O., Herzog, G. F., Marti, K., & Caffee, M. W. 2006, in Meteorites and the Early Solar System II, ed. D. S. Lauretta & H. Y. McSween, 829
Farley, K. A., Vokrouhlický, D., Bottke, W. F., & Nesvorný, D. 2006, Nature, 439, 295
Golubov, O. & Krugly, Y. N. 2012, ApJ, 752, L11

Gradie, J. C., Chapman, C. R., & Tedesco, E. F. 1989, in Asteroids II, ed. R. P. Binzel, T. Gehrels, & M. S. Matthews, 316–335
Graf, T. & Marti, K. 1994, Meteoritics, 29, 643
Graf, T. & Marti, K. 1995, J. Geophys. Res., 100, 21247
Granvik, M., Morbidelli, A., Jedicke, R., et al. 2018, Icarus, 312, 181
Greenberg, R. 1982, AJ, 87, 184
Greenwood, R. C., Schmitz, B., Bridges, J. C., Hutchison, R., & Franchi, I. A. 2007, Earth and Planetary Science Letters, 262, 204
Haack, H., Farinella, P., Scott, E. R. D., & Keil, K. 1996, Icarus, 119, 182
Harris, A. W., Boslough, M., Chapman, C. R., et al. 2015, Asteroid Impacts and Modern Civilization: Can We Prevent a Catastrophe?, 835–854
Harris, A. W. & Chodas, P. W. 2021, Icarus, 365, 114452
Heck, P. R., Schmitz, B., Bottke, W. F., et al. 2017, Nature Astronomy, 1, 0035
Hendler, N. P. & Malhotra, R. 2020, Planet. Sci. J., 1, 75
Holsapple, K. A. 2007, Icarus, 187, 500
Knežević, Z. & Milani, A. 2003, A&A, 403, 1165
Korochantseva, E. V., Trieloff, M., Lorenz, C. A., et al. 2007, Met. Planet. Sci., 42, 113
Levison, H. F. & Duncan, M. J. 1994, Icarus, 108, 18
Love, S. G. & Brownlee, D. E. 1993, Science, 262, 550
Marchi, S., McSween, H. Y., O'Brien, D. P., et al. 2012, Science, 336, 690
Marsset, M., Brož, M., Vernazza, P., et al. 2020, Nature Astronomy, 4, 569
Marsset, M., DeMeo, F. E., Burt, B., et al. 2022, AJ, 163, 165
Marsset, M. & et al. submit., Nature Astronomy
Marti, K. & Graf, T. 1992, Annual Review of Earth and Planetary Sciences, 20, 221
Marzari, F., Davis, D., & Vanzani, V. 1995, Icarus, 113, 168
Molnar, L. A. & Haegert, M. J. 2009, in AAS/Division for Planetary Sciences Meeting Abstracts, Vol. 41, AAS/Division for Planetary Sciences Meeting Abstracts #41, 27.05
Morbidelli, A., Bottke, W. F., Nesvorný, D., & Levison, H. F. 2009, Icarus, 204, 558
Moskovitz, N., Schottland, R., Burt, B., et al. 2019, in EPSC-DPS Joint Meeting 2019, Vol. 2019, EPSC–DPS2019–644
Nesvorný, D. & Bottke, W. F. 2004, Icarus, 170, 324
Nesvorný, D., Bottke, W. F., Vokrouhlický, D., et al. 2008, ApJ, 679, L143
Nesvorný, D., Brož, M., & Carruba, V. 2015, Identification and Dynamical Properties of Asteroid Families, ed. P. Michel, F. E. DeMeo, & W. F. Bottke (Univ. Arizona Press), 297–321
Nesvorný, D., Jenniskens, P., Levison, H. F., et al. 2010, ApJ, 713, 816
Nesvorný, D., Vokrouhlický, D., Bottke, W. F., & Sykes, M. 2006, Icarus, 181, 107
Nesvorný, D., Vokrouhlický, D., Morbidelli, A., & Bottke, W. F. 2009, Icarus, 200, 698
Novaković, B. & Radović, V. 2019, in EPSC-DPS Joint Meeting 2019, Vol. 2019, EPSC–DPS2019–1671
Nugent, C. R., Mainzer, A., Masiero, J., et al. 2015, ApJ, 814, 117
O'Brien, D. P., Marchi, S., Morbidelli, A., et al. 2014, Planet. Space Sci., 103, 131
Parker, A., Ivezić, Ž., Jurić, M., et al. 2008, Icarus, 198, 138
Quinn, T. R., Tremaine, S., & Duncan, M. 1991, AJ, 101, 2287
Reach, W. T., Franz, B. A., & Weiland, J. L. 1997, Icarus, 127, 461
Rubin, A. E. 1994, Meteoritics, 29, 93
Rubincam, D. P. 2000, Icarus, 148, 2
Russell, C. T., Raymond, C. A., Coradini, A., et al. 2012, Science, 336, 684
Schmitz, B., Peucker-Ehrenbrink, B., Lindström, M., & Tassinari, M. 1997, Science, 278, 88
Schmitz, B., Tassinari, M., & Peucker-Ehrenbrink, B. 2001, Earth and Planetary Science Letters, 194, 1
Ševeček, P., Brož, M., Nesvorný, D., et al. 2017, Icarus, 296, 239
Ševeček, P., Brož, M., Čapek, D., & Ďurech, J. 2015, MNRAS, 450, 2104
Šidlichovský, M. & Nesvorný, D. 1996, Celestial Mechanics and Dynamical Astronomy, 65, 137
Swindle, T. D., Kring, D. A., & Weirich, J. R. 2014, Geological Society of London Special Publications, 378, 333
Sykes, M. V. 1990, Icarus, 85, 267
Terfelt, F. & Schmitz, B. 2021, Proceedings of the National Academy of Science, 118, e2020977118
Thomas, C. A. & Binzel, R. P. 2010, Icarus, 205, 419
Usui, F., Kuroda, D., Müller, T. G., et al. 2011, PASJ, 63, 1117
Vernazza, P., Binzel, R. P., Thomas, C. A., et al. 2008, Nature, 454, 858
Vernazza, P., Brož, M., Drouard, A., et al. 2018, A&A, 618, A154
Vernazza, P., Ferrais, M., Jorda, L., et al. 2021, A&A, 654, A56
Vernazza, P., Zanda, B., Binzel, R. P., et al. 2014, ApJ, 791, 120
Vokrouhlický, D. 1998, A&A, 335, 1093
Vokrouhlický, D., Bottke, W. F., & Nesvorný, D. 2017, AJ, 153, 172
Vokrouhlický, D., Brož, M., Bottke, W. F., Nesvorný, D., & Morbidelli, A. 2006a, Icarus, 183, 349
Vokrouhlický, D., Brož, M., Bottke, W. F., Nesvorný, D., & Morbidelli, A. 2006b, Icarus, 182, 118
Vokrouhlický, D., Brož, M., Novaković, B., & Nesvorný, D. 2021, A&A, 654, A75
Vokrouhlický, D. & Farinella, P. 1999, AJ, 118, 3049
Zappalà, V., Bendjoya, P., Cellino, A., Farinella, P., & Froeschlé, C. 1995, Icarus, 116, 291

Appendix A: Parameters of the principal bodies

Hereinafter, we discuss preferred values of parameters. (4) Vesta has a volume-equivalent diameter 525 km and a volumetric density $3.456\,\mathrm{g\,cm^{-3}}$ (Russell et al. 2012); the parent body size is practically the same as Vesta.

(20) Massalia is 132 km in diameter (Usui et al. 2011) and its density is $3.71\,\mathrm{g\,cm^{-3}}$ (Carry 2012), although with a 20% uncertainty.

For (170) Maria, (808) Merxia, (847) Agnia, (158) Koronis, (1272) Gefion, we used diameters 35 km, 33 km, 30 km, 34 km (Usui et al. 2011), and just 6.9 km (Nugent et al. 2015), even though Gefion is not the largest remnant, it just has the lowest designation. Because the densities are unknown, we assumed $3\,\mathrm{g\,cm^{-3}}$. All of these breakups were catastrophic disruptions; parent body size is substantially larger, i.e., 125 km, 50 km, 52 km, 161 km, and 72 km, respectively. This is important for the velocity field. We determined these values by scaling of synthetic SFDs of Durda et al. (2007); uncertainties are of the order of 10 %

(832) Karin is 14.3 km in diameter (Usui et al. 2011), and the family parent body size is up to 36 km.

For (3) Juno, we used 254 km, $3.15\,\mathrm{g\,cm^{-3}}$, according to Vernazza et al. (2021). It is the 2nd largest S-type asteroid.

For (8) Flora, 146 km, $2.43\,\mathrm{g\,cm^{-3}}$ from the same reference. If about half of the family members has been lost in the ν_6 resonance the parent body size might have been larger.

Finally, (15) Eunomia is 256 km in diameter, and its density $2.96\,\mathrm{g\,cm^{-3}}$ is close the mean density of S-types (Usui et al. 2011; Vernazza et al. 2021). It is the 1st largest S-type asteroid.

Appendix B: Family ages

Previous orbital modelling, cratering record, or meteorite radiometry can be used to estimate the age of an asteroid family. The Vesta family is constrained by the Rheasylvia basin on Vesta, or *in situ* observations (Marchi et al. 2012; O'Brien et al. 2014), as (1000 ± 200) My. It is in agreement with our collisional model (Tab. 2).

The Phocaea family was studied by Carruba (2009); it is up to 2200 My old, as inferred from the Yarkovsky drift rates. Its SFD indicates a younger age (cf. Tab. 2).

The Massalia family is (152 ± 18) My old according to Vokrouhlický et al. (2006b). Parameters of the velocity field were also estimated, $v_5 = 24\,\mathrm{m\,s^{-1}}$, $D_5 = 5\,\mathrm{km}$, $v \propto D^{-1}$. On contrary, its shallow SFD indicates an older age.

The Maria family may be up to 3000 ± 1000 My old, according to (a_p, H) distribution (Brož et al. 2013).

The Merxia family, (330 ± 50) My old (Vokrouhlický et al. 2006b), is almost certainly young, having a smooth and steep SFD from the LR to the observational incompleteness.

The Agnia family is (100 ± 25) My old (Vokrouhlický et al. 2006a), again smooth and steep.

On contrary, the Koronis family is really old, (2500 ± 1000) My (Brož et al. 2013). Koronis is probably even older than Maria, because the 'break' of the SFD is at larger D's (3 vs. 5 km).

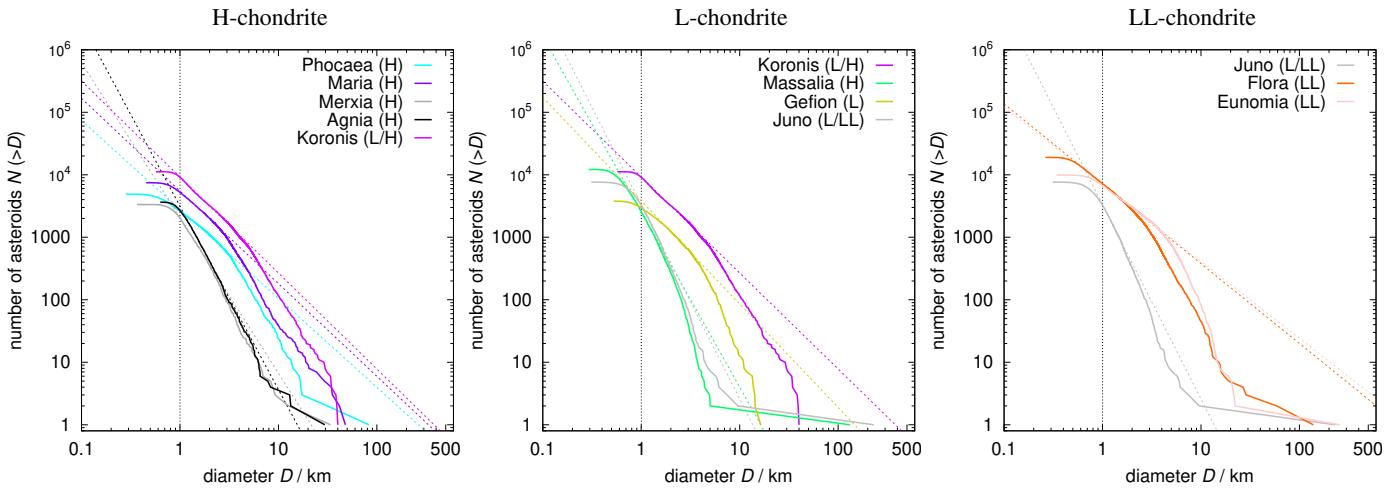

Fig. 1. Observed cumulative size-frequency distributions (SFDs) of the S-type asteroid families: H-chondrite-like (left), L-chondrite-like (middle), and LL-chondrite-like (right). Each group is dominated by one or two families, but it sensitively depends on the respective diameter D. For reference, $D = 1$ km is indicated (black dotted line). The SFDs exhibit the following features: largest remnant (LR), possibly an intermediate-size fragment, largest fragment (LF), first slope (q_1), which is steep, starting at the LF, second slope (q_2), which is shallow, related to long-term collisional evolution, third slope (q_3), which is even shallower, related to the scaling law and observed break in the main belt SFD, fourth slope (q_4) or bend-off, related to observational incompleteness. (see Tab. 1). Alternatively, q_4 may be related to a mass conservation. Extrapolations to sub-km sizes are also indicated (colour dotted lines), however, a collisional model is preferred for this purpose (cf. Fig. 5).

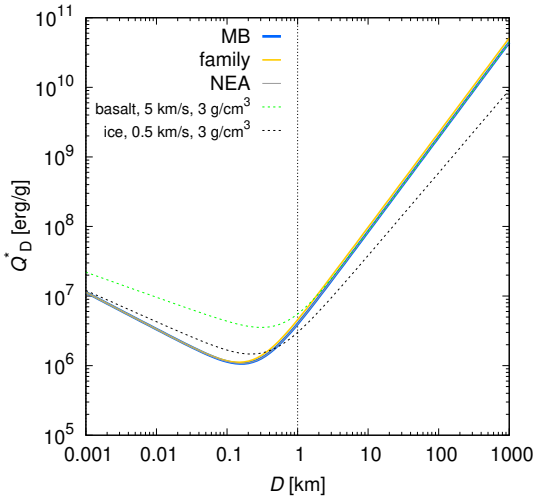

Fig. 2. Modified scaling law $Q^\star(D)$ used in our collisional model. A comparison to the nominal scaling law for basalt at 5 km/s (green line) from Benz & Asphaug (1999) is also plotted. This modification is needed to fit the main belt SFD at sub-km sizes.

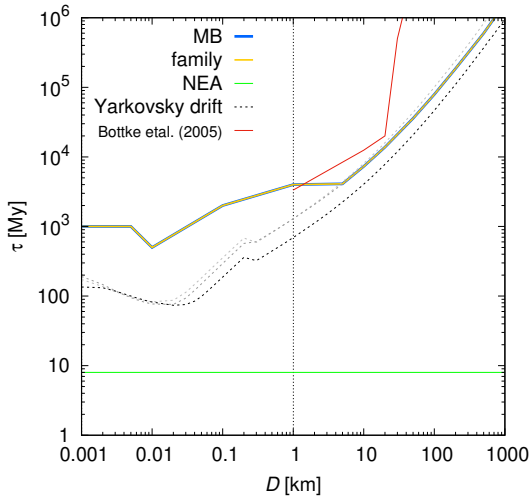

Fig. 3. Dynamical decay time scales $\tau(D)$ used in our collisional model. The main belt and families have relatively long time scales, which are needed to fit the NEO population, being transported from the main belt and having a short time scale (8 My). A comparison to the nominal time scale (red line) of Bottke et al. (2005) is also plotted. For the Yarkovsky drift without spin axis evolution, decay would be significantly shorter.

The Gefion family is constrained by radiometry of LL chondrites (467 ± 2) My (Greenwood et al. 2007; Nesvorný et al. 2009), and compatible with the Yarkovsky/YORP model. On contrary, its SFD is shallow, which indicates an older age.

For the Juno family, we assume (750 ± 150) My, according to Carruba & Nesvorný (2016).

The Flora family was estimated to be (1200 ± 200) My old (Vokrouhlický et al. 2017). Our N-body modelling suggests that the synthetic family should be more extended, with a substantially larger $D_{\rm PB} > 146$ km. About half of bodies was lost in the ν_6 resonance.

Finally, the Eunomia family is probably (3200 ± 1000) My old (Carruba & Nesvorný 2016). Our N-nody modelling suggests a range 1880 up to 3300 My on the basis of the $(a_{\rm p}, e_{\rm p})$ distribution. It almost reaches a steady state, because we recalibrate the synthetic SFD to the observed SFD in every time step, which is then insensitive to the decay of the population Brož & Morbidelli (2013). Eunomia is most likely older than Flora (cf. the 'break').

Appendix C: Selection of 'slow' shapes.

In our orbital model, we noted a strong dynamical selection of shapes, which evolve slowly due to the YORP torque (Fig. C.1).

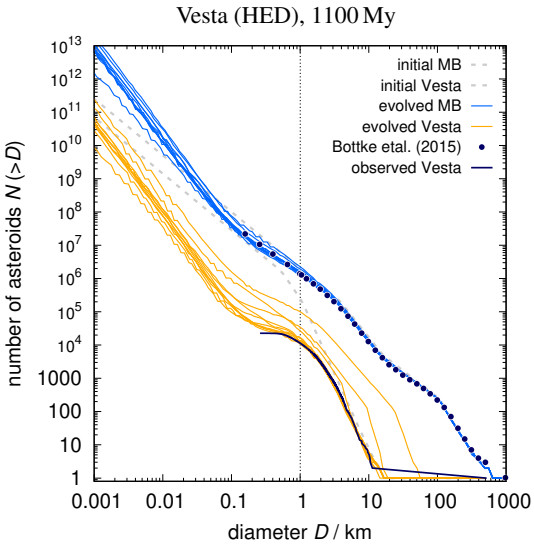

Fig. 4. Synthetic SFD of the main belt and the Vesta family, used for calibration. The age 1100 ± 100 My is consistent with O'Brien et al. (2014).

If the shape is fast, the critical frequency is reached fast, this shape is changed to another one, and *vice versa*.

Out of 200 nominal shapes from Čapek & Vokrouhlický (2004), e.g., 185, 101, 129, 106, 58, ... are slow (see Fig. C.2). They seem to be more round, but it is generally difficult to recognize it. They should be less like a wind-mill (Rubincam 2000).

Moreover, the scaling relation we use in our model:

$$c = c_{\mathrm{YORP}} \left(\frac{a}{a_0}\right)^{-2} \left(\frac{R}{R_0}\right)^{-2} \left(\frac{\rho}{\rho_0}\right)^{-1} \qquad \text{(C.1)}$$

where $a_0 = 2.5$ au, $R_0 = 1$ km, $\rho_0 = 2.5\,\mathrm{g\,cm^{-3}}$, is not complete. A scaling with the rotation period (or frequency) is missing. While the nominal period $P_0 = 6$ h, for which the torques were originally computed, is too long for meteoroids, the YORP effect should work even in the limit of zero conductivity (Rubincam 2000). It implies a negligible dependence on the rotation period. This may change, if a transversal heat diffusion in mm- to cm-scale surface features is properly taken into account (Golubov & Krugly 2012; Ševeček et al. 2015). However, it would require a dedicated computation of the YORP effect for metre-sized bodies.

Appendix D: Supplementary tables

The intrinsic collisional probability and the mean collisional velocity were computed with Greenberg (1982) theory for precessing orbits. The values for various combinations of populations are listed **in** Tabs. D.1, D.2. **The flux of meteoroids originating from families, accounting for various collisional probabilities with the Earth, is listed in Tab. D.3.**

Appendix E: Supplementary figures

We show the outcome of families identification procedure and a preferred extent of the families in Fig. E.1.

Table D.1. Intrinsic collisional probability and the mean collisional velocity for various main belt populations.

populations	p	v
–	$10^{-18}\,\mathrm{km^{-2}\,y^{-1}}$	$\mathrm{km\,s^{-1}}$
MB–MB	2.860	5.772
MB–Agnia	4.466	4.471
MB–Eunomia	3.347	5.784
MB–Flora	2.736	5.667
MB–Gefion	3.545	5.115
MB–Juno	3.009	6.491
MB–Koronis	4.657	4.271
MB–Maria	2.923	6.095
MB–Massalia	4.269	5.042
MB–Merxia	4.057	4.744
MB–Phocaea	2.419	8.252
MB–Vesta	2.919	5.288
Agnia–Agnia	10.535	2.241
Eunomia–Eunomia	5.961	5.725
Flora–Flora	15.506	4.235
Gefion–Gefion	5.913	4.352
Juno–Juno	4.950	7.034
Karin–Karin	14.865	1.531
Koronis–Koronis	13.323	1.625
Maria–Maria	7.112	5.866
Massalia–Massalia	29.009	4.234
Merxia–Merxia	8.235	3.571
Phocaea–Phocaea	5.936	10.307
Vesta–Vesta	12.601	3.613

Table D.2. Same as Tab. D.1 for the Earth and meteoroids in the NEO space.

populations	p	v
–	$10^{-18}\,\mathrm{km^{-2}\,y^{-1}}$	$\mathrm{km\,s^{-1}}$
Earth–Agnia	120.524	24.672
Earth–Eunomia	46.952	24.992
Earth–Flora	44.860	21.663
Earth–Gefion	123.191	21.484
Earth–Juno	47.467	23.907
Earth–Karin	76.386	25.567
Earth–Koronis	115.815	19.872
Earth–Maria	49.847	27.295
Earth–Massalia	18.955	21.341
Earth–Merxia	43.796	19.474
Earth–Phocaea	9.306	31.419
Earth–Vesta	49.352	22.963

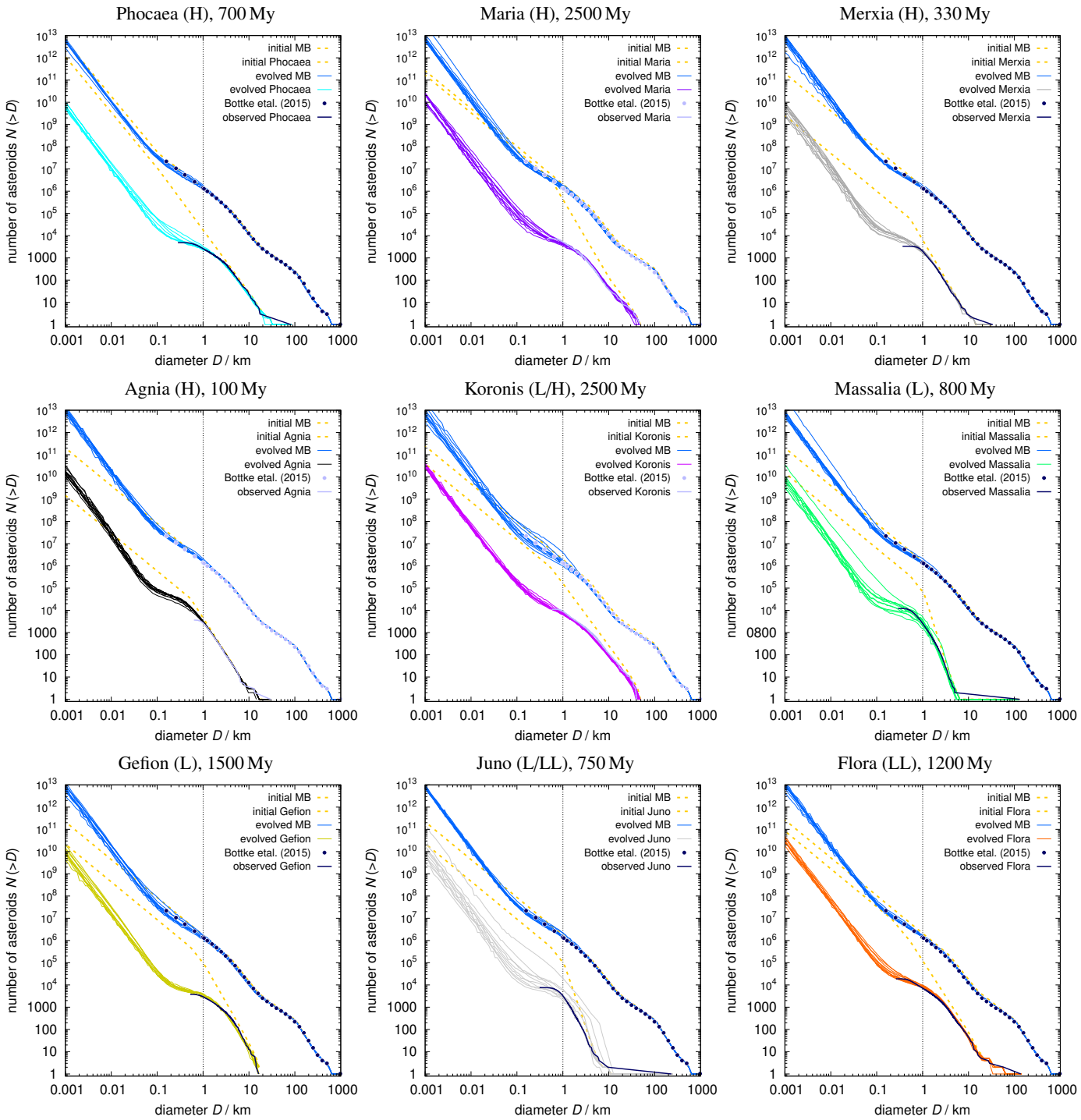

Fig. 5. Synthetic SFDs of the S-type asteroid families derived from our collisional model. Every panel contains: the initial main belt, the initial family (yellow dotted), evolved main belt (blue), evolved family (different colours), observed main belt (Bottke et al. 2015), observed family (gray solid). The SFDs between 1 and 10 km were initially a smooth power-law. They evolved due to collisions and exhibit a characteristic slope change at about 5 km, which is observed (see Tab. 1). Every model was run 10 times to account for stochasticity. The best-fit age is reported on top (see Tab. 2).

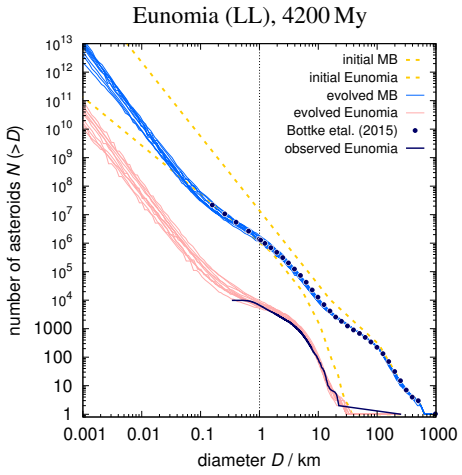

Fig. 6. continued.

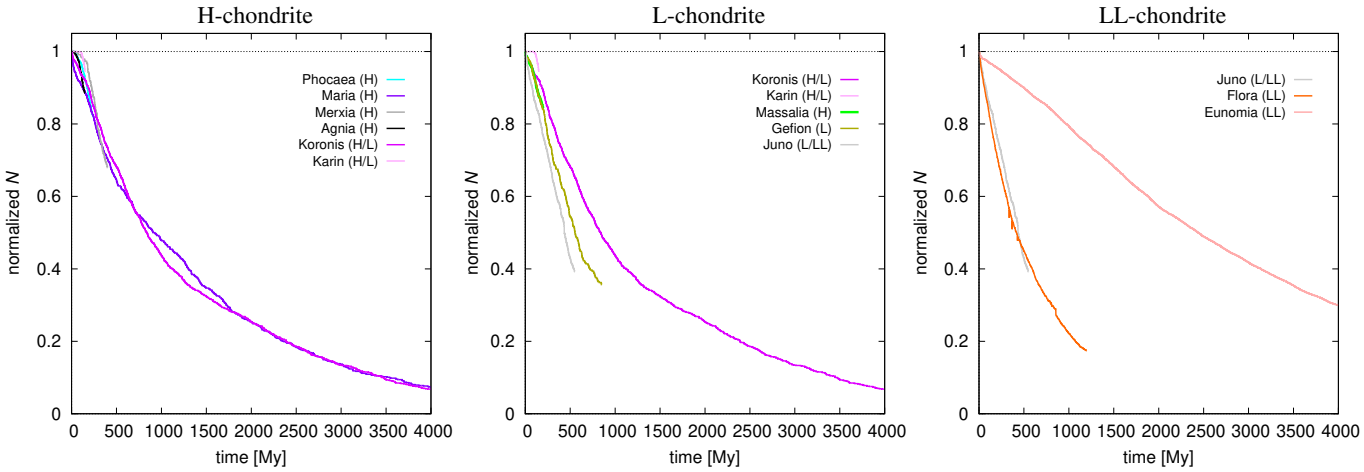

Fig. 7. Dynamical decay of selected synthetic asteroid families derived from our orbital model: H-chondrite-like (left), L-chondrite (middle), LL-chondrite (right). Normalized number of bodies vs. time is plotted. The decay is induced by gravitational resonances, the Yarkovsky drift, as modified by the YORP effect, collisional reorientations, and limited by the critical frequency. Sizes of bodies correspond to the observed SFDs; most of them are kilometre-sized.

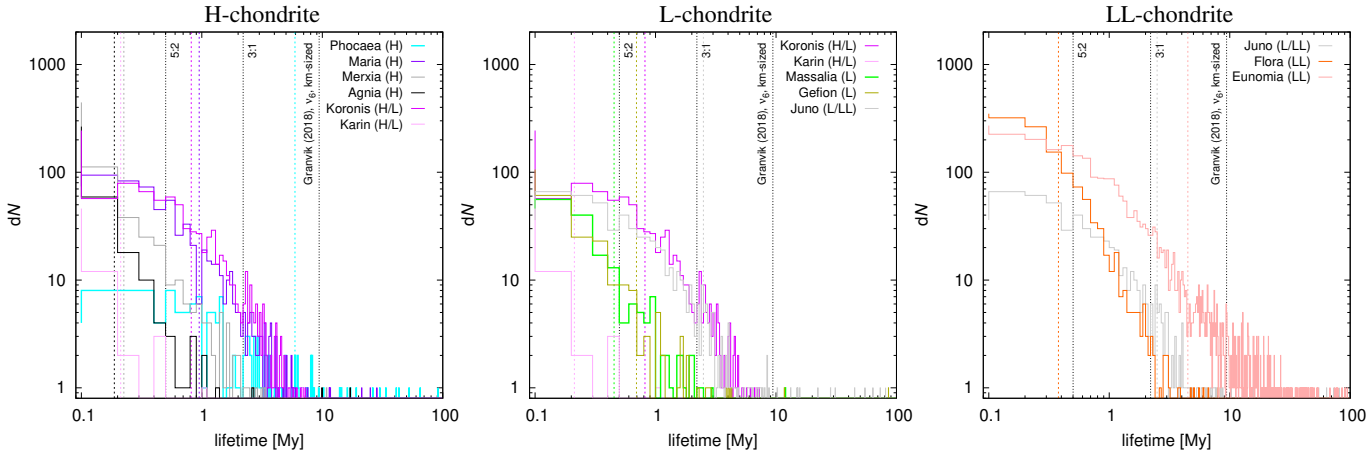

Fig. 8. Lifetimes of bodies in the NEO space derived from our orbital model: H-chondrite-like (left), L-chondrite (middle), LL-chondrite (right). When bodies escape from the respective families via resonances (cf. Fig. E.1), they temporarily enter the NEO space. Their lifetimes are different for different resonances, where low-order or outer-main-belt ones tend to produce short-lived orbits, and *vice versa*. The mean (*not* median) lifetimes are plotted for each family (colour dashed). For comparison, the lifetimes from Granvik et al. (2018) (9.4, 2.2, 0.5 My for the ν_6, 3:1, 5:2 resonances; see their Tab. 3) are also plotted (black dotted).

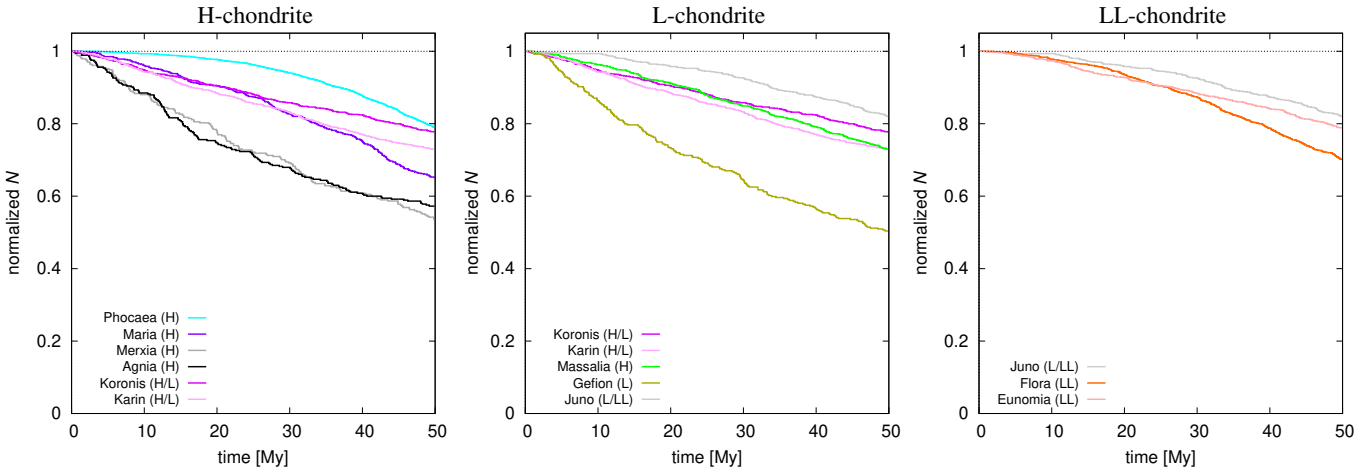

Fig. 9. Same as Fig. 7, but for metre-sized bodies.

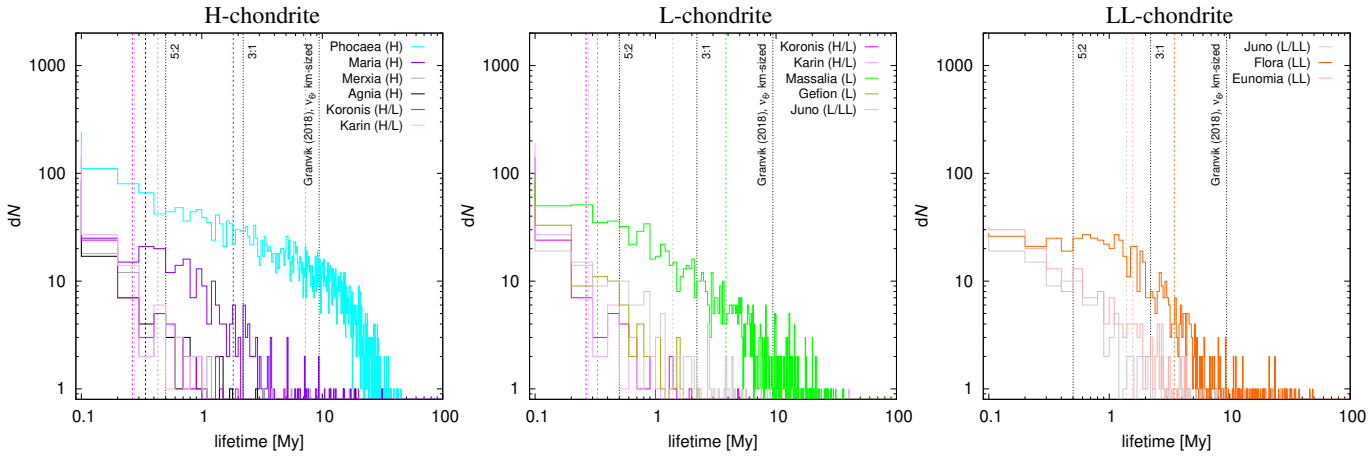

Fig. 10. Same as Fig. 8, but for metre-sized bodies.

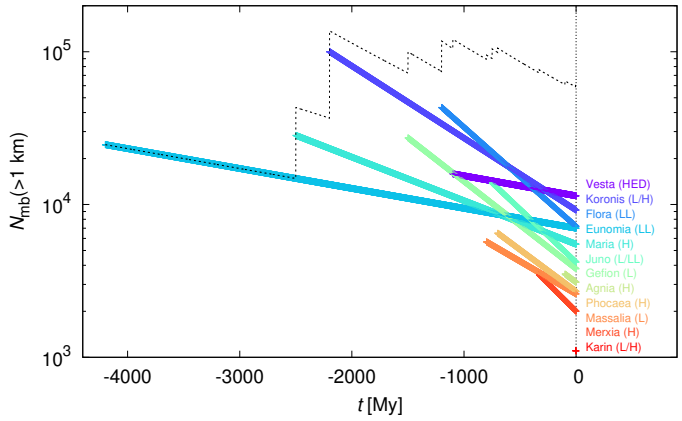

Fig. 11. Extrapolated contributions of asteroid families to the population of kilometre-sized bodies in the main belt. The observed number $N_{\rm mb}(>1\,{\rm km})$ is on the right ($t = 0$). Here we account for the dynamical decay only (see Tab. 4; column $\tau_{\rm mb}$), so that at the family origin ($t = t_0$) the population was large and decayed as $\exp(-(t - t_0)/\tau_{\rm mb})$. The total of all selected families is indicated (dashed line). The total of all main belt bodies is 1.36×10^6.

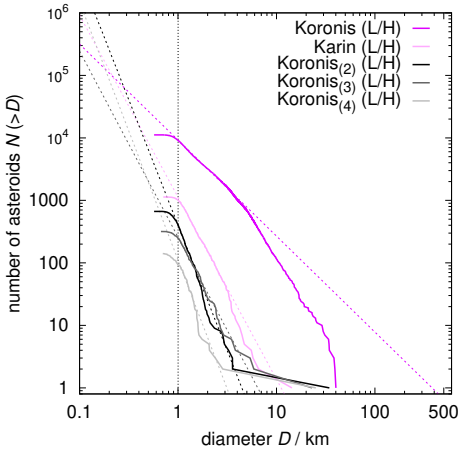

Fig. 12. Same as Fig. 1 for the Karin, Koronis$_{(2)}$, Koronis$_{(3)}$, Koronis$_{(4)}$ families.

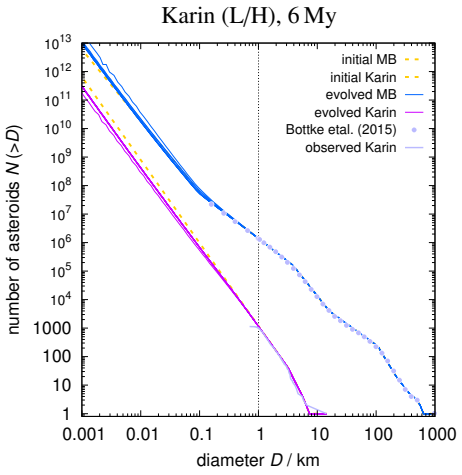

Fig. 13. Same as Fig. 5 for the Karin family.

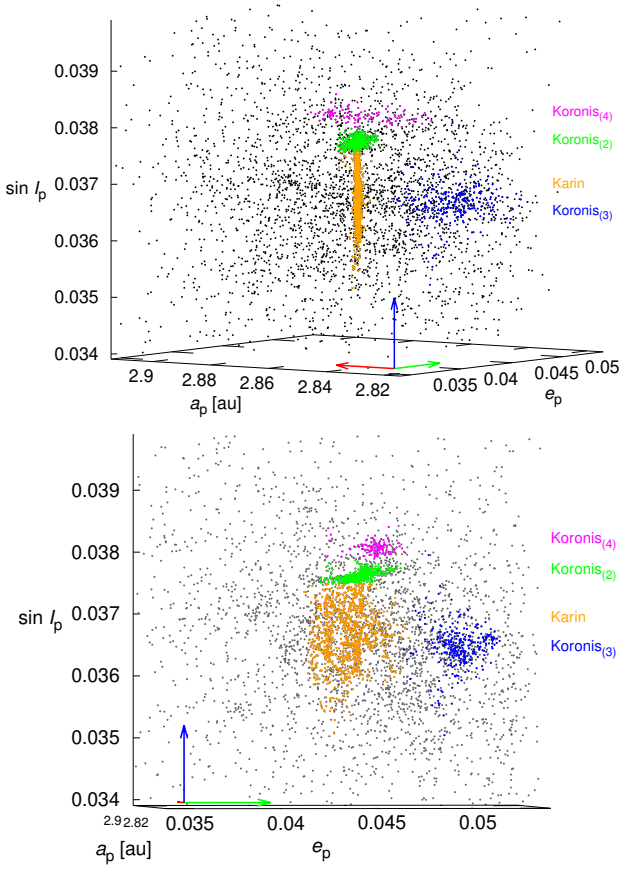

Fig. 14. The Karin collisional series in the space of proper elements ($a_{\rm p}, e_{\rm p}, \sin I_{\rm p}$). Top: A view from a suitable oblique direction, when the Karin (orange) and the Koronis$_{(2)}$ (green) families appear as the most compact clusters. Bottom: A view from another direction (rotated ←), when two 'new' clusters — provisionally designated Koronis$_{(3)}$ (blue) and Koronis$_{(4)}$ (magenta) — appear as compact. Probably, they are associated to asteroids (1289) Kutaissi and (321) Florentina, respectively. They are actually older and extended along the semimajor axis $a_{\rm p}$ due to the Yarkovsky effect, but they remained compact in both the eccentricity $e_{\rm p}$ and inclination $\sin I_{\rm p}$. These principal directions are also indicated by arrows.

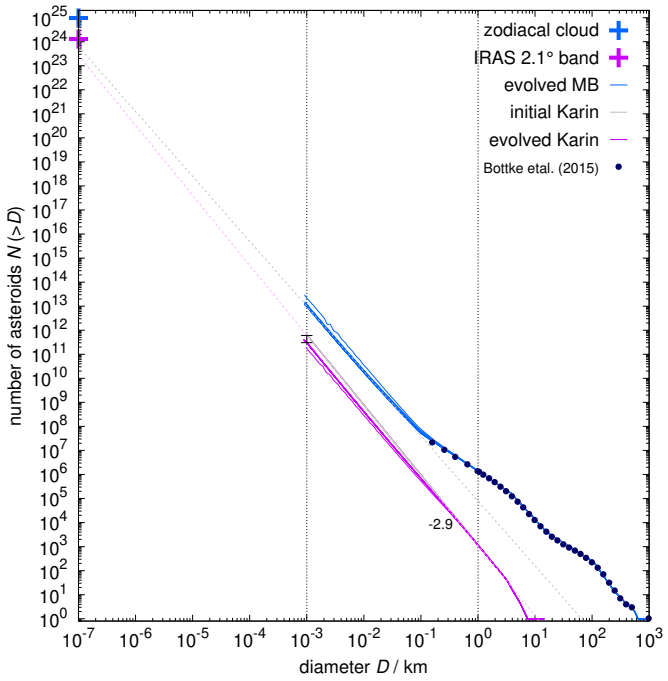

Fig. 15. Synthetic SFD of the Karin family extrapolated down to 100 μm with the slope −2.9. The value of $N(>100\,\mu\mathrm{m}) = 1.3 \times 10^{24}$ particles, inferred from the 2.1° dust band, is indicated by a cross. **The interpolated population of metre-sized bodies is indicated by an error bar.** For comparison, the **main belt** and the zodiacal cloud value **(without dust from Jupiter-family comets; Nesvorný et al. 2010)** are plotted.

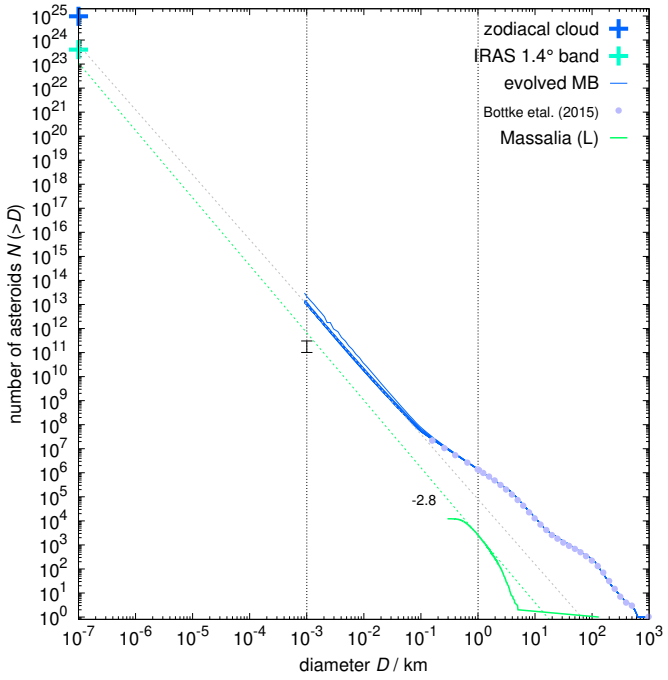

Fig. 16. Same as Fig. 15, for the Massalia family.

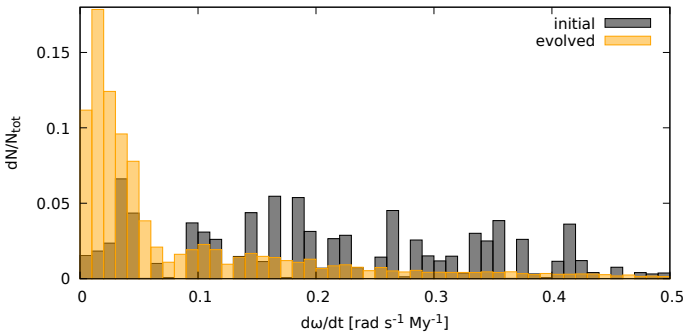

Fig. C.1. Normalized differential distribution $\mathrm{d}N/N_{\mathrm{tot}}$ of spin accelerations $\mathrm{d}\omega/\mathrm{d}t$ (in rad s^{-1} My^{-1}) for a population of metre-sizes bodies originated from the Agnia family; close to the initial conditions (black) and evolved due to the YORP effect (orange). A strong preference for 'slow' shapes is evident.

Table D.3. Meteoroid flux $\Phi = pN_{\mathrm{neo}}$.

family	Φ
–	10^{-9} km^{-2} y^{-1}
Vesta (HED)	21.5-75.1
Phocaea (H)	3.0-5.9
Maria (H)	7.4-18.5
Merxia (H)	0.7-2.1
Agnia (H)	4.0-8.0
Koronis (L/H)	3.0-6.0
Karin (L/H)	29.6-59.3
Massalia (L)	2.1-5.2
Gefion (L)	2.6-7.9
Juno (L/LL)	1.6-4.8
Flora (LL)	28.1-56.3
Eunomia (LL)	3.7-22.1
HED	21.5-75.1
H	28.0-56.3
L	6.3-17.9
LL	31.8-78.4
H+L+LL	66.1-152.6
S types	1200?
all bodies	3900[C]

Notes. [C] Ceplecha (1992)

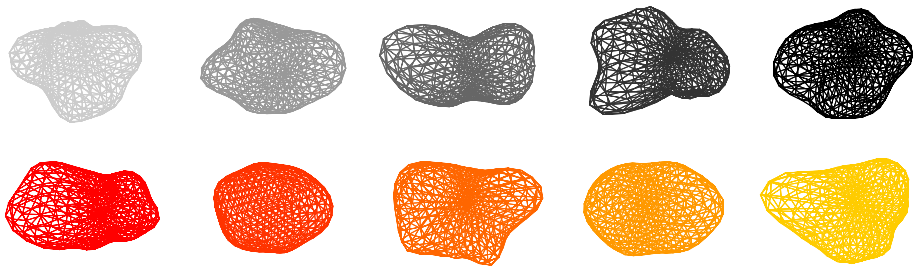

Fig. C.2. Examples of shapes from Čapek & Vokrouhlický (2004), which exhibit fast (top) vs. slow (bottom) evolution of the spin rate due to the YORP effect. The latter appear to be more round, but it is generally difficult to recognize a shape exhibiting a large vs. small YORP torque.

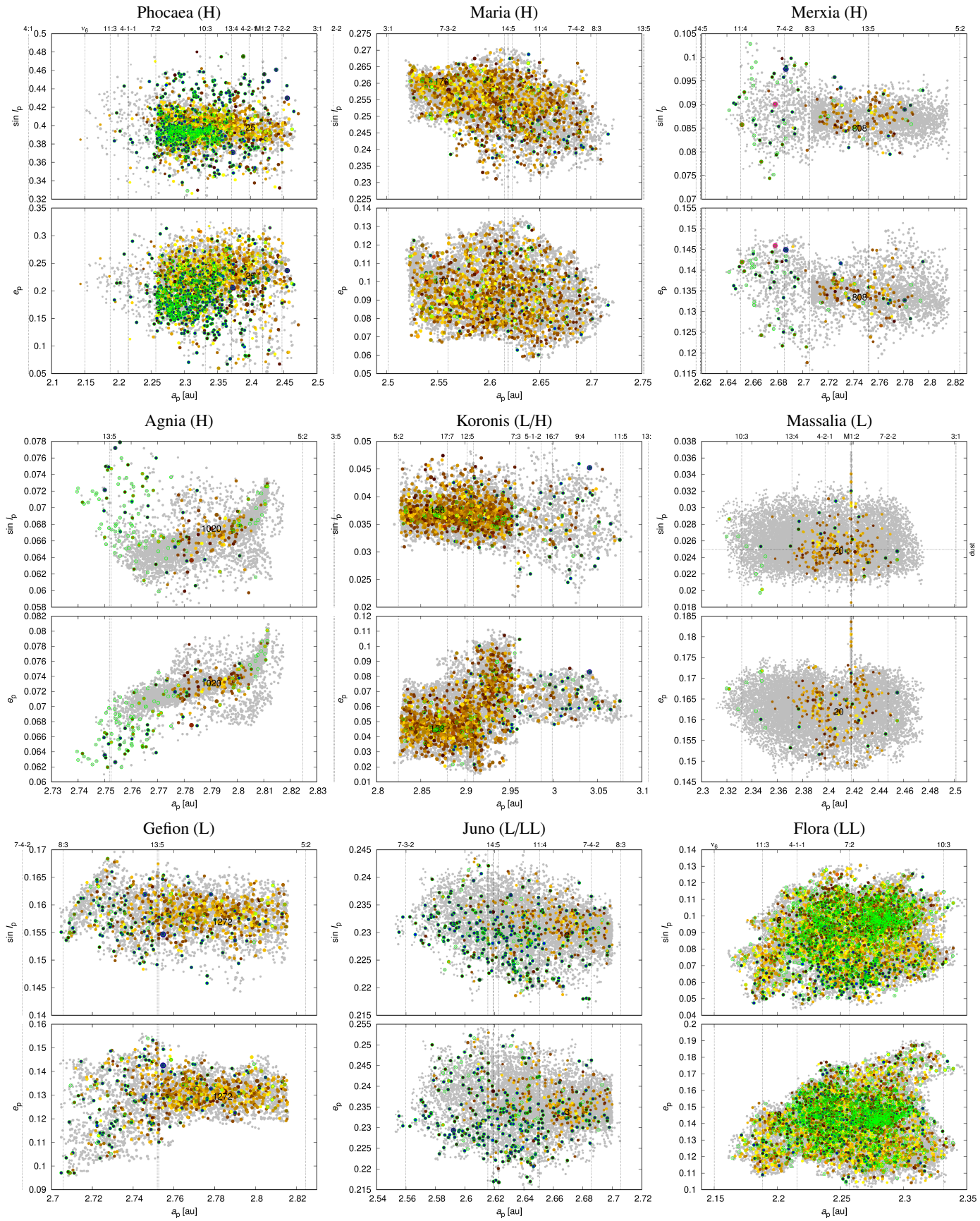

Fig. E.1. S-type families as identified in this work. The proper semimajor axis a_p vs. the proper eccentricity e_p and vs. the proper inclination $\sin I_p$ are plotted. Colours correspond to the geometric albedo p_V (blue → yellow). Major mean-motion and three-body resonances (**vertical** dotted lines), as well as identified interlopers (green circles) are indicated. **Some of the bodies ((20) Massalia, (832) Karin) have inclinations corresponding to the IRAS dust bands (horizontal dotted lines).**

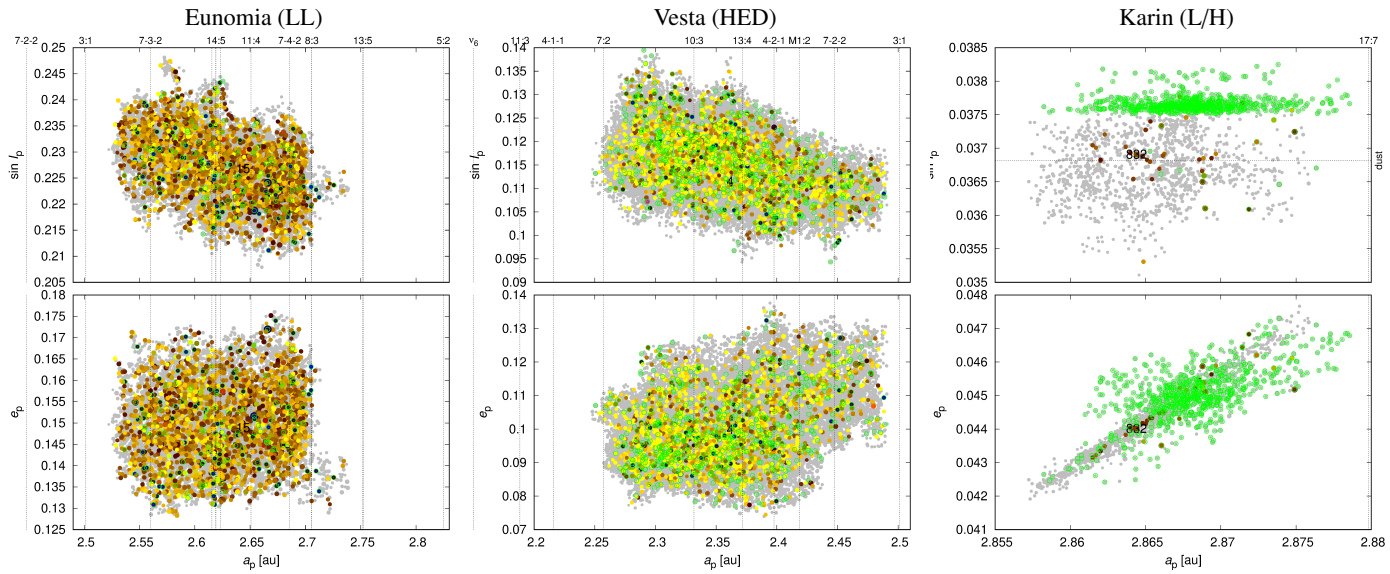

Fig. E.1. continued.